Somatic genetics analysis of sleep in adult mice

Guodong Wang[1,2,3,10], Qi Li[1,2,10], Junjie Xu[1,2,4], Shuai Zhao[5], Rui Zhou[1,2,6], Zhenkang Chen[7], Wentong Jiang[1,2,3], Xue Gao[1,2], Shuang Zhou[1,2,4], Zhiyu Chen[1,2], Quanzhi Sun[1,2], Chengyuan Ma[8], Lin Chen[1,2], Bihan Shi[1,2], Ying Guo[1,2], Haiyan Wang[1,2], Xia Wang[1,2], Huaiye Li[1,2], Tao Cai[1,2], Yibing Wang[1,2], Zhineng Chen[5], Fengchao Wang[1,2*] & Qinghua Liu[1,2,9*]

[1]National Institute of Biological Sciences (NIBS), Beijing 102206, China; [2]Tsinghua Institute of Multidisciplinary Biomedical Research, Tsinghua University, Beijing 102206, China; [3]Graduate School of Peking Union Medical College, Chinese Academy of Medical Sciences, Beijing 100730, China; [4]College of Life Sciences, Beijing Normal University, Beijing 100875, China; [5]Institute of Automation, Chinese Academy of Sciences, Beijing 100080, China; [6]College of Biological Sciences, China Agriculture University, Beijing 100094, China; [7]Children's Medical Center Research Institute, UT Southwestern Medical Center, Dallas, TX 75235, USA; [8]Chinese Institute of Brain Science, Beijing 102206, China; [9]International Institute for Integrative Sleep Medicine (WPI-IIIS), University of Tsukuba, Tsukuba 305-8575, Japan.

[10]These authors contributed equally to this study

[Running Title: Somatic genetics analysis of sleep in adult mice]

[Key words: adult brain chimeric (ABC), AAV-PHP.eB, knockout (KO), somatic genetics analysis, Cre/loxP recombination, CRISPR/Cas9, sleep phenotypes]

* Corresponding authors:

liuqinghua@nibs.ac.cn (lead contact); wangfengchao@nibs.ac.cn

25 **GRAPHIC ABSTRACT**

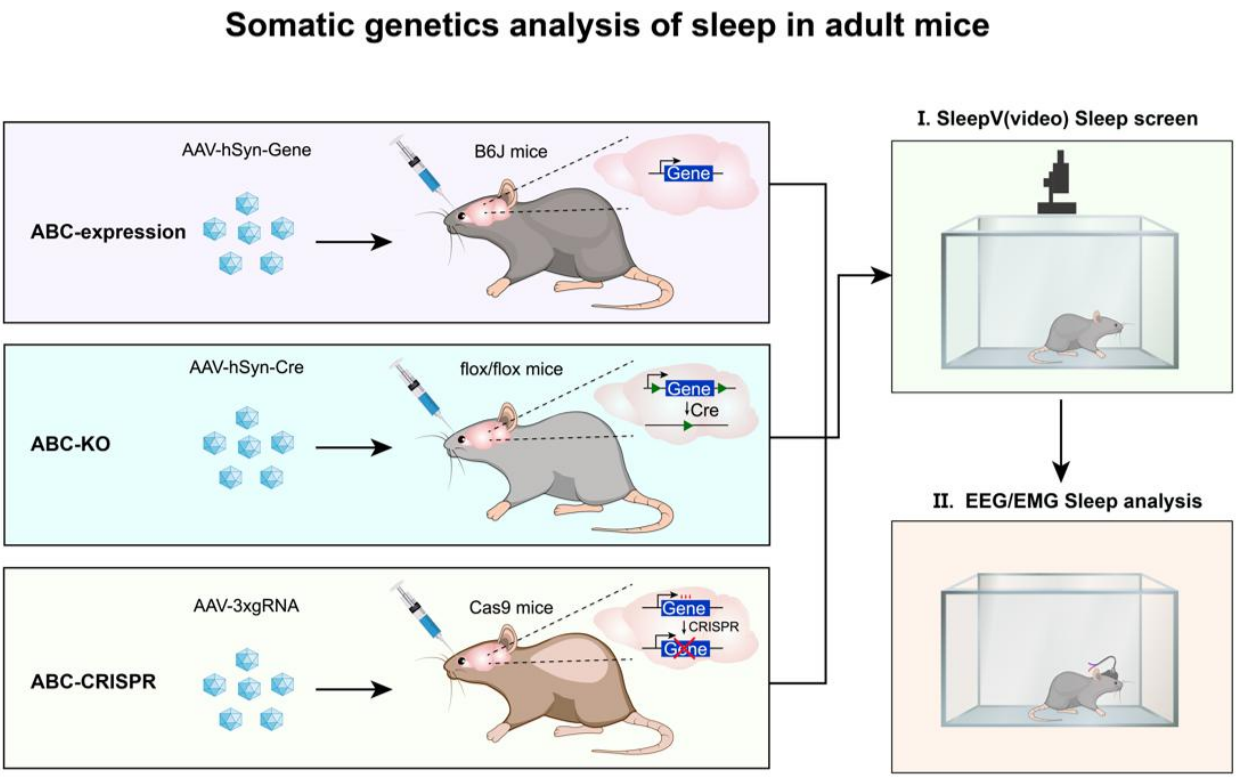

26

27

28 **HIGHLIGHT**

29 1. A simple adult brain chimeric (ABC) platform for somatic genetics analysis of sleep genes;

30 2. A highly accurate and non-invasive SleepV (video) system for high-throughput sleep screening;

31 3. ABC-KO by AAV-Cre injection facilitates systematic sleep screening of conditional flox mice;

32 4. ABC-KO by CRISPR/Cas9 enables one-step analysis of redundant sleep genes in adult mice;

33

34

35

36

37

38

SUMMARY

The molecular mechanisms of mammalian sleep regulation remain largely unknown. Classical forward and reverse mouse genetic approaches require germline mutations and, thus, are unwieldy to study the sleep functions of essential genes or redundant pathways. It is also costly and time-consuming to conduct large-scale electroencephalogram (EEG)/electromyogram (EMG)-based mouse sleep screening due to lengthy genetic crosses and labor-intensive surgeries. Here, we develop a highly efficient adult brain chimeric (ABC) expression/knockout (KO) platform and a highly accurate AI-augmented SleepV (video) system for high-througphut somatic genetics analysis of sleep in adult mice. This ABC platform involves intravenous administration of adeno-associated viruses (AAV) that bypass the blood brain barrier and transduce the majority of adult brain neurons. Constitutive or inducible ABC-expression of CREB and CRTC1 reduces both quantity and quality of non-rapid-eye-movement sleep (NREMS), whereas ABC-KO of CREB by AAV-mediated Cre/loxP recombination increases daily NREMS amount. Moreover, ABC-KO of exon 13 of *Sik3* by AAV-Cre injection of *Sik3-E13*$^{flox/flox}$ adult mice phenocopies *Sleepy* (*Sik3*$^{Slp/Slp}$) mice, which carry a germline splicing mutation resulting in skipping of exon 13 of *Sik3*. While both long and short isoforms of SLP kinase contribute to, ABC-KO of *Slp* allele by CRISPR/Cas9 rescues the hypersomnia of *Sik3*$^{Slp/+}$ mice. Double ABC-KO of orexin/hypocretin receptors by CRISPR/Cas9 results in chocolate-induced narcolepsy episodes. We envision that these somatic genetics approaches should facilitate efficient and sophisticated studies of many brain-related cellular, physiological and behavioral processes in adult mice without genetic crosses.

62 **INTRODUCTION**

63 Although sleep exists ubiquitously in animals, the molecular mechanisms of sleep
64 regulation in mammals remain largely unknown. Forward genetics screening of randomly
65 mutagenized mice is a powerful and hypothesis-free approach to identify key sleep regulatory
66 genes in mammals (Banks et al., 2020; Funato et al., 2016; Kapfhamer et al., 2002; Takahashi et al.,
67 1994). On the other hand, reverse genetics, through the making of transgenic, knockout (KO) and
68 knockin mice for specific genes of interest, represents a hypothesis-driven approach to identify and
69 characterize new sleep regulatory genes (Graves et al., 2003; Hellman et al., 2010; Honda et al.,
70 2018; Mikhail et al., 2017; Takahashi et al., 1994). This latter approach is greatly expedited by next
71 generation gene-editing technologies, such as the clustered regularly interspaced short palindromic
72 repeats (CRISPR)/Cas9 system (Hsu et al., 2014; Sunagawa et al., 2016; Tatsuki et al., 2016; Wang
73 et al., 2013). However, it is very costly and time-consuming to conduct large-scale mouse sleep
74 screening for two main reasons: 1) both forward and reverse genetics approaches require germline
75 mutations and, thus, genetic crosses; 2) the electroencephalogram (EEG)/electromyogram (EMG)-
76 based sleep analysis requires labor-intensive and invasive surgery.

77 Accumulating evidence suggest that sleep is essential for survival in invertebrate and
78 vertebrate animals (Bentivoglio and Grassi-Zucconi, 1997; Rechtschaffen et al., 1989; Shaw et al.,
79 2002; Vaccaro et al., 2020). Thus, it is plausible that core sleep regulatory genes may be essential
80 for survival in mice. It is estimated that about one third of ~23,000 mammalian genes are essential
81 genes (Dickinson et al., 2016), which often encode structural proteins, housekeeping enzymes, or
82 complex signaling proteins with critical roles at multiple stages of development (Tian et al., 2018).
83 However, classical mouse genetics approaches are unwieldy to study the sleep functions of these
84 essential genes owing to the early lethality caused by germline mutations. In some cases, forward
85 or reversed genetics may identify viable gain-of-function or partial loss-of-function mutations that
86 can uncover the sleep phenotypes of essential genes (Funato et al., 2016; Graves et al., 2003).

87 Conditional KO mice are commonly used to bypass early lethality and analyze the temporal
88 and/or tissue-specific functions of essential genes (Gierut et al., 2014). Typically, this strategy
89 involves crossing of tissue-specific Cre-expressing transgenic mice with conditional flox mice that
90 contain two loxP sites flanking a critical exon(s) of the target gene (Gierut et al., 2014). The
91 Cre/loxP-mediated site-specific recombination will exercise the critical exon(s) and disrupt the
92 target gene in a tissue-specific and/or temporal manner. However, this strategy is time-consuming
93 (1 to 2 years) by requiring not only the appropriate Cre transgenic and flox mouse strains, but also
94 multiple genetic crosses to generate sufficient number of conditional knockout mice for
95 comprehensive sleep analysis (Gierut et al., 2014).

96 Given the central importance of sleep in physiology and survival, it is likely that redundant
97 pathways exist for sleep regulation. Thus, genetic ablation of a gene of interest may cause mild or
98 no sleep phenotype because of genetic redundancy. Additionally, mice with germline mutations
99 have ample time to adapt or compensate for sleep phenotypes before the EEG/EMG-based sleep
100 analysis normally conducted at the adult stage. Moreover, it is a costly and tedious process to
101 generate double or triple knockout mice *via* classical germline genetics approaches (Sunagawa et
102 al., 2016). A combination of triple-target CRISPR and modified embryonic stem cell technologies
103 allows for biallelic knockout of multiple genes in a single generation for sleep analysis, however,
104 only when the double or triple knockout mice are viable (Sunagawa et al., 2016).

105 Recombinant adeno-associated viruses (AAV) have been widely used as vehicles for gene
106 expression, knockdown/knockout and gene therapy in the central nervous system (CNS) (Borel et
107 al., 2014; Suzuki et al., 2016; Yang et al., 2016). To bypass the blood-brain barrier (BBB) and
108 restrict gene expression, these applications often require local AAV injection into specific regions
109 of the mouse brain. Alternatively, intravenous injection of AAVs provides a non-invasive strategy
110 for systemic gene delivery into the CNS (Choudhury et al., 2016; Deverman et al., 2016; Foust et
111 al., 2009). Notably, Cre-recombination-based AAV-targeted evolution (CREATE) has been used to

112 isolate two AAV9 variants, AAV-PHP.B and AAV-PHP.eB, which can efficiently bypass BBB in
113 certain mouse strains and systemically transduce neurons and astrocytes across the adult mouse
114 brain and spinal cord (Chan et al., 2017; Deverman et al., 2016).

115 Here, we used AAV-PHP.eB to develop an adult brain chimeric (ABC) platform for rapid,
116 efficient and sophisticated somatic genetics analysis of sleep genes in adult mice. We demonstrated
117 that the ABC-expression platform, coupled with a highly accurate SleepV (video) system, could
118 facilitate high-throughput screening of sleep genes. On the other hand, we developed ABC-KO by
119 AAV-mediated Cre/loxP recombination to facilitate systematical screening of conditional flox mice
120 for sleep phenotypes. Moreover, multiplex ABC-KO by triple-target CRISPR/Cas9 could enable
121 one-step analysis of redundant sleep genes. These somatic genetics approaches should greatly
122 facilitate the elucidation of the core sleep regulatory pathways, including essential or redundant
123 genes, in adult mice without genetic crosses.

124

125 **RESULTS**

126 **Development of ABC platform for somatic genetics analysis of sleep genes in adult mice**

127 Sleep and wake are two alternate physiological states of the brain, which globally impact
128 the molecular, synaptic and cellular activities across the whole brain (Cirelli and Tononi, 1998; de
129 Vivo et al., 2017; Diering et al., 2017; Elliott et al., 2014; Tononi and Cirelli, 2014; Wang et al.,
130 2018). Thus, homeostatic sleep regulation likely involves the majority of neurons and possibly
131 astrocytes across the adult mouse brain (Tononi and Cirelli, 2014; Wang et al., 2018). It has
132 recently been reported that retro-orbital injection of 10^{11} vector genomes (vg) of single-stranded
133 AAV-PHP.eB systemically transduced the majority of brain neurons, including 69% of cortical
134 neurons and 55% of striatal neurons in the adult mouse (Chan et al., 2017). Therefore, we
135 hypothesized that AAV-PHP.eB-mediated adult brain chimeric (ABC)-expression of sleep
136 regulatory genes should in theory result in significant sleep phenotypes **(Figure 1A)**.

137 To verify the efficiency of this AAV delivery system, we performed retro-orbital injection
138 of 12-week old C57BL/6J mice with dual AAV-PHP.eB (10^{12} vg/mice) viruses, AAV-CBh-Cre and
139 AAV-EF1α-DIO-H2B-eGFP **(Figure 1B)**. In this experiment, only brain neurons transduced with
140 both viruses could exhibit Cre-dependent expression of histone H2B-eGFP fusion protein. As
141 shown by co-immunostaining of GFP and NeuN **(Figures 1C and 1D)**, both viruses efficiently co-
142 transduced the majority of adult brain neurons three weeks after AAV administration.
143 Quantification of double positive neurons showed high rates of viral transduction across eight
144 different brain regions, ranging from 56.6% in the hippocampus to 88.7% in the thalamus **(Figure**
145 **1D)**. Furthermore, ABC-expression of GFP from the pan-neuronal human synapsin (hSyn)
146 promoter did not affect the sleep-wake architecture as compared to no virus injected control mice
147 **(Figures S1A-S1C)**. These results suggest that it should be feasible to use the ABC-expression
148 platform to screen for sleep regulatory genes.
149
150 **A highly accurate, AI-augmented SleepV system for high-throughput sleep screening**
151 The EEG/EMG recording is the gold standard method for analysis of the sleep-wake
152 architecture in mammals (Lo et al., 2004; Weiergraber et al., 2005). Based on the different patterns
153 of electrical signals, each short (4 to 20-s) epoch of EEG/EMG data is annotated into one of three
154 states: wakefulness (wake), rapid eye movement sleep (REMS), or non-rapid eye movement sleep
155 (NREMS). NREMS, which occupies the majority (~90%) of total sleep in mice, is characterized by
156 high percentage of the delta (1-4 Hz) power of EEG spectrum. The delta power of NREMS
157 measures the sleep quality/depth and is regarded as the best known measurable index of
158 homeostatic sleep need (Franken et al., 2001).
159 However, this EEG/EMG method is not suitable for high-throughput sleep screening
160 because it requires labor-intensive and invasive surgery to implant electrodes into the skull and
161 muscle and extensive (≥ 2 weeks) recovery time from surgery before EEG/EMG recording.

162 Moreover, the semi-automated sleep staging software only has ~90% accuracy and requires
163 intensive efforts to manually correct the annotation of several days of EEG/EMG data per mouse.
164 On the other hand, a number of non-invasive sleep monitoring systems have been developed and
165 utilized for mouse sleep analysis, including the infrared video recording system (Banks et al., 2020;
166 Fisher et al., 2012; Pack et al., 2007), the piezoelectric system tracking mouse movement (Flores et
167 al., 2007; Yaghouby et al., 2016) and the plethysmography system monitoring the respiration of
168 mouse (Sunagawa et al., 2016).

169 To facilitate high-throughput sleep screening, we developed an artificial intelligence (AI)-
170 enhanced video-based sleep monitoring system that we named SleepV, which used a novel pattern
171 recognition algorithm to classify the sleep/wake states based on inactivity/activity of the mouse
172 **(Figures 1A and S1D)**. First, our algorithm uses Gaussian filtering, adaptive and global
173 thresholding to extract from every image frame (25 frames/sec) the suspected regions of interest
174 (ROI), which are then judged to be a mouse or not by a pre-trained deep neural network **(Figure**
175 **S1D)**. Second, to determine whether the mouse is active or not, the algorithm calculates a high
176 confidence difference score for the mouse between "t" and "t+m" frames by integrating the
177 network prediction score (predict), the mouse mask area (Intersection of Union, IoU) and the gray
178 information (color) within the detected mask **(Figure S1D and S1E)**. Finally, SleepV defines the
179 sleep state as ≥ 40-s of continuous immobility and, to accommodate subtle mouse movements
180 during sleep, annotates ≤ 15-s of activity in between two sleep states as sleep.

181 To evaluate the performance of SleepV, we coupled infrared video recording with
182 EEG/EMG recording to examine the accuracy of our fully automated sleep staging software.
183 According to the hourly plot of sleep time of six adult male mice **(Figure 1E)**, we found that the
184 accuracy of sleep/wake staging by SleepV was comparable to that of EEG/EMG analysis.
185 Moreover, there was a 95-99% epoch-by-epoch agreement of sleep/wake staging between the two
186 methods, although SleepV cannot distinguish between NREMS and REMS **(Figure 1F)**. The

accuracy of our SleepV system was significantly higher than the 88-94% accuracy of previously reported video-based sleep monitoring systems (Banks et al., 2020; Fisher et al., 2012; Pack et al., 2007). Next, we used SleepV to record the sleep/wake cycles of fifty-nine C57BL/6J adult mice for three consecutive days. The distribution of daily sleep time measured by SleepV in these mice was comparable to that of EEG/EMG analysis in previous studies **(Figure S1F**) (Funato et al., 2016; Wang et al., 2018). Moreover, SleepV could easily distinguish the hypersomnia phenotype of *Sleepy* (*Sik3*$^{Slp/+}$) mice, which showed ~210 min increase in daily sleep time relative to wild-type littermates **(Figures S1G and S1H)**. These results indicate that SleepV is a highly accurate, non-invasive and automatic sleep monitoring system suitable for high-throughput sleep screening.

A pilot ABC-expression sleep screen of synaptic plasticity regulators

Accumulating studies suggest a close link between synaptic plasticity and sleep need regulation. The fruit flies raised in socially enriched environment sleep for significantly longer time than those raised in isolation (Donlea et al., 2009; Ganguly-Fitzgerald et al., 2006). Learning experience also increase sleep need in both flies and mammals, manifested by increased sleep time and/or NREMS delta power (Donlea et al., 2009; Ganguly-Fitzgerald et al., 2006; Huber et al., 2006; Huber et al., 2004). By comparative phosphoproteomic analysis of *Sleepy* and sleep-deprived mouse brains, we recently identified 80 sleep need index phosphoproteins (SNIPPs), of which the majority are annotated synaptic proteins, including many regulators of synaptic plasticity (Wang et al., 2018).

To test our hypothesis that changing synaptic plasticity could lead to changes in sleep need, we combined the ABC-expression platform with the SleepV system to conduct a pilot sleep screen of eleven known synaptic plasticity regulators **(Figure 1A)**. These regulators of synaptic plasticity included the immediate early gene products ARC and Homer1a (Chowdhury et al., 2006; Diering et al., 2017; Hu et al., 2010; Plath et al., 2006; Shepherd et al., 2006), cyclin-dependent kinase 5

212 (CDK5) (Bibb, 2003), synaptic vesicle protein Rab3a (Kapfhamer et al., 2002), dominant negative
213 form of polo-like kinase 2 (Plk2-dn) (Seeburg et al., 2008), Ca^{2+}/calmodulin-dependent protein
214 kinase II (CamKIIα/β) and IV (CamKIV) (Ibata et al., 2008; Lisman et al., 2012) and activity-
215 dependent transcriptional factors cyclic AMP-response element binding protein (CREB), cAMP-
216 regulated transcriptional coactivator 1 (CRTC1) and constitutively active MEF2-VP16–a fusion
217 protein between the DNA binding domain of MEF2 and the VP16 transactivation domain (Benito
218 and Barco, 2010; Ch'ng et al., 2012; Flavell et al., 2006; Kandel, 2012; Nonaka et al., 2014). As
219 shown by co-immunostaining of HA-tag and NeuN, intravenous administration of AAV-PHP.eB
220 consistently resulted in systemic expression of individual gene in approximately 40-80% of the
221 adult brain neurons **(Figure 1G)**. Although ABC-expression of most genes had little effect on the
222 sleep/wake cycle, this pilot screen identified two potential hits, CREB and CRTC1, which
223 significantly reduced daily sleep time **(Figure 1H)**.

224 CREB is a well-known transcriptional activator that consists of an amino (N)-terminal
225 transactivation domain as well as a carboxy (C)-terminal basic leucine zipper (bZIP) DNA-binding
226 and dimerization domain (Dash et al., 1990). CREB binds as a dimer to the cAMP response
227 elements (CRE), which contain a palindromic (TGACGTCA) or half-site (TGACG or CGTCA)
228 sequence, in the promoter or enhancer regions of many target genes (Comb et al., 1986; Montminy
229 et al., 1986; Short et al., 1986). Alternative splicing results in multiple protein isoforms of CREB,
230 of which the α and Δ isoforms, but not the β isoform, show high affinity for CRE sites (Ruppert et
231 al., 1992). Phosphorylation of CREBα at serine 133 (or $CREB_{\Delta}$ at serine 119) by cAMP-dependent
232 protein kinase (PKA) is critical for the recruitment of coactivators, including the histone acetyl
233 transferases CBP/p300 and transcriptional activation of certain target genes (Chrivia et al., 1993;
234 Gonzalez and Montminy, 1989; Shaywitz and Greenberg, 1999). Alternatively, CREB functions in
235 tandem with CRTCs, also known as transducers of regulated CREB activity coactivators (TORCs),
236 to activate the transcription of specific target genes (Conkright et al., 2003; Iourgenko et al., 2003).

237

238 **ABC-expression of CREB and/or CRTC1 reduces NREMS amount and delta power**

239 Next, we performed EEG/EMG recording to further characterize the sleep phenotypes
240 caused by ABC-expression of $CREB_{\Delta}$. It has been shown that serine 133 to alanine (S133A)
241 phosphor-mutation of $CREB_{\alpha}$ prevents transcriptional activation of specific target genes (Chrivia
242 et al., 1993; Gonzalez and Montminy, 1989). Thus, we also examined the sleep phenotypes of
243 ABC-expression of phosphor-mutant $CREB_{\Delta}^{S119A}$ in adult mice. Co-immunostaining revealed that
244 intravenous administration of AAV-hSyn-$CREB_{\Delta}$ or AAV-hSyn-$CREB_{\Delta}^{S119A}$ resulted in efficient
245 transduction of 40-80% of cortical and thalamic neurons **(Figures 2A and 2B)**. Relative to ABC-
246 eGFP mice, both ABC-$CREB_{\Delta}$ and ABC-$CREB_{\Delta}^{S119A}$ mice exhibited on average ~120 min
247 decrease in daily NREMS amount accompanied by reduced NREMS delta power, which occurred
248 predominantly during the dark phase **(Figures 2C-E and S2C-D)**. These results suggest that ABC-
249 expression of $CREB_{\Delta}$ reduces NREMS amount and delta power in a manner independent of S119
250 phosphorylation.

251 Because CRTC1 enhanced the transcriptional activity of CREB (Conkright et al., 2003;
252 Iourgenko et al., 2003), we asked whether ABC-co-expression of $CREB_{\Delta}$ and CRTC1 could result
253 in additive sleep phenotypes as compared to ABC-expression of either $CREB_{\Delta}$ or CRTC1 alone. In
254 contrast to nuclear localization of $CREB_{\Delta}$ or $CREB_{\Delta}^{S119A}$, CRTC1 was predominantly localized in
255 the cytoplasm **(Figure 2A)**. Relative to ABC-eGFP mice, ABC-CRTC1 mice exhibited a ~47 min
256 decrease in daily NREMS time accompanied by reduced NREMS delta power during the dark
257 phase **(Figures 2F-H and S2F-S2J)**. It should be noted that SleepV overestimated the reduction of
258 sleep time in ABC-CRTC1 mice by mistaking frequent muscle twitching during sleep as waking in
259 these mice **(Figure S2K)**. Importantly, ABC-co-expression of $CREB_{\Delta}$ and CRTC1 resulted in
260 enhanced sleep phenotypes: ~150 min decrease in daily NREMS time accompanied by further
261 reduced NREMS delta power during the dark phase **(Figures 2F-2H)**. Taken together, these results

262 demonstrate that the combination of ABC-expression platform and highly accurate SleepV system
263 can facilitate high-throughput screening of sleep regulatory genes in adult mice.
264
265 **Inducible ABC-expression of CREB^{VP16} and/or CRTC1^{CA} causes strong sleep phenotypes**
266 ABC-expression of constitutively active CREB^{VP16}–a fusion protein between the DNA-
267 binding domain of CREB and VP16 transactivation domain (Barco et al., 2002)–resulted in
268 lethality in C57BL/6J adult mice one week after AAV injection. Similarly, ABC-expression of
269 constitutively active CRTC1^{CA} containing two (S151A and S245A) phosphor-mutations, also
270 resulted in lethality one week after AAV injection. Therefore, we used a Tet-on inducible system to
271 express CREB^{VP16} or CRTC1^{CA} in the adult mouse brains by injection of two AAV-PHP.eB viruses
272 expressing rtTA from the EF1α promoter and CREB^{VP16} or CRTC1^{CA} from the TRE promoter,
273 respectively **(Figures 3A and 3B)**. There was little difference in the baseline sleep-wake
274 architecture among the inducible (i) ABC-eGFP, iABC-CREB^{VP16} and iABC-CRTC1^{CA} mice when
275 transcription from the TRE promoter was shut off by binding of rtTA in the absence of
276 Doxycycline (Dox) (data not shown). On the other hand, the expression of GFP, CREB^{VP16}, or
277 CRTC1^{CA} was rapidly induced in the brain cells of these mice within three days after drinking Dox-
278 containing water **(Figures 3B, 3C and S3A, S3B)**. Interestingly, there appeared to be a slight
279 circadian shift of the sleep/wake cycle at the light/dark transition among all mice possibly due to
280 the effects of Dox **(Figures 3D-3O)**. While ABC-induction of GFP did not affect the total
281 sleep/wake time, ABC-induction of CREB^{VP16} or CRTC1^{CA} caused progressive decrease in the
282 daily amounts of NREMS and REMS accompanied by corresponding increase in wake time during
283 the three days of Dox treatment **(Figures 3D-3O and S3C-S3N)**. Remarkably, ABC-CRTC1^{CA}
284 mice were almost constantly awake as shown by 91.8% and 97.1% reduction in NREMS and
285 REMS amounts, respectively, on day 3 of Dox treatment relative to the baseline sleep amounts
286 before Dox treatment **(Figures 3L-3O and S3K-S3N)**. These results suggest that the iABC-

287 expression system can be used to study the sleep phenotypes of genes, of which constitutive
288 expression will lead to lethality in adult mice.
289
290 **ABC-KO of CREB by Cre/loxP recombination increases daily NREMS amount**
291 *Creb1* is an essential gene of which complete ablation results in perinatal lethality in mice
292 (Bleckmann et al., 2002). A partial *Creb1* knockout strain, in which the α and Δ isoforms of CREB
293 are deleted, is homozygous viable and exhibits ~100 min increase of daily NREMS time (Graves et
294 al., 2003). Moreover, forebrain-specific knockout of *Creb1* in the excitatory neurons similarly
295 increases daily NREMS amount (Wimmer et al., 2020). To generate ABC-$Creb1^{KO}$ mice, we retro-
296 orbitally injected $Creb1^{flox/flox}$ mice with AAV-PHP.eB expressing mCherry or Cre recombinase
297 from the pan-neuronal hSyn promoter, respectively. Immunoblotting revealed that the level of
298 CREB expression was reduced by ~50% in whole brain lysates of AAV-hSyn-Cre injected mice
299 relative to AAV-hSyn-mCherry injected mice **(Figures 4A-4C)**. Because CREB was also
300 expressed in the astrocytes that could not be targeted by neuron-specific Cre expression (Pardo et
301 al., 2017), ABC-$Creb1^{KO}$ was likely to occur in greater than 50% of the adult brain neurons. In
302 accordance with previous studies (Graves et al., 2003; Wimmer et al., 2020), ABC-$Creb1^{KO}$ mice
303 exhibited ~100 min increase in daily NREMS amount, but with no significant change in NREMS
304 delta power **(Figures 4D-4F)**. These results suggest that loss of CREB expression in most adult
305 brain neurons can result in a significant sleep phenotype.
306
307 **ABC-KO of exon 13 of *Sik3* phenocopies *Sleepy* mice**
308 Forward genetics screening recently identified a *Sleepy* ($Sik3^{Slp/+}$) mouse strain, in which a
309 5' splicing mutation causes the skipping of exon 13 of *Sik3* gene and, hence, an in-frame deletion
310 of 52 amino acids from SIK3–an AMP-activated protein kinase (AMPK)-related kinase (Funato et
311 al., 2016). The *Sleepy* ($Sik3^{Slp/+}$) mice exhibit on average ~250 min increase in daily NREMS time

312 and constitutively elevated NREMS delta power relative to wild-type littermates (Funato et al.,
313 2016). It remains unclear, however, whether the hypersomnia of *Sik3*$^{Slp/+}$ mice is the primary
314 phenotype owing to direct effects of SLP kinases, or the secondary phenotype resulting from
315 developmental abnormalities of the brain or dysfunctions of other peripheral organs.

316 To distinguish among these possibilities, we performed retro-orbital injection of AAV-
317 hSyn-Cre into the *Sik3-E13*$^{flox/flox}$ mice, in which the Cre/loxP-mediated excision of exon 13 of *Sik3*
318 would convert the *Sik3-E13*^{flox} allele into a functionally equivalent *Sleepy* (*Sik3-E13*$^{\Delta}$) allele
319 **(Figure 4G)**. Immunoblotting estimated that mutant SLP kinases were expressed in at least 40% of
320 the adult brain neurons following AAV-hSyn-Cre injection **(Figures 4H and 4I)**. Remarkably,
321 ABC-KO of exon 13 of *Sik3* in adult mice induced a strong hypersomnia phenotype similar to that
322 of *Sleepy* mice carrying the germline *Slp* mutation, manifested by ~200 to 300 min increase in daily
323 NREMS time accompanied by constitutively elevated NREMS delta power **(Figures 4J-4L and**
324 **S4F-S4J)**. These results strongly suggest that the hypersomnia of *Sleepy* mice is the primary
325 phenotype resulting from mutant SLP kinases directly affecting the sleep regulatory machinery in
326 the adult brain neurons.

327

328 **ABC-expression of Slp-S causes mild hypersomnia in a kinase-dependent manner**

329 The mouse *Sik3* gene encodes multiple protein isoforms owning to alternative splicing
330 (Funato et al., 2016). Additionally, immunoblotting of whole brain lysates prepared from *Sik3*$^{+/+}$,
331 *Sik3*$^{Slp/+}$ and *Sik3*$^{Slp/Slp}$ mice detected a new prominent ~72 kDa short isoform of SIK3/SLP (SIK3-
332 S/SLP-S) **(Figure 5B)**. Surprisingly, the annotated SIK3-S isoform in the genome database lacks
333 the N-terminal 58 amino acids, including lysine 37 that is required for ATP binding and kinase
334 activity of SIK3 (Katoh et al., 2006). By reverse transcription (RT)-PCR and sequencing, we
335 verified that the endogenous *Sik3/Slp-S* mRNA contained the sequence encoding the N-terminal 58
336 amino acids **(Figures 5C and S5A)**.

337 It remains unclear how different SLP isoforms contribute to the hypersomnia of *Sik3*$^{Slp/+}$
338 mice and whether this phenotype is dependent on the kinase activity of SLP proteins. To address
339 these important questions, we performed ABC-expression of HA-tagged GFP, Slp-S, or Slp-S^{K37M}
340 in C57BL/6J adult mice **(Figure S5A)**. Despite of similar AAV transduction rates, the expression
341 of Slp-S or Slp-S^{K37M} was significantly lower than that of GFP in the mouse brain **(Figures S5B**
342 **and S5C)**. As compared to ABC-eGFP mice, ABC-Slp-S mice exhibited ~60 min increase in daily
343 NREMS time accompanied by a marked increase in NREMS delta power **(Figures 5D-5F)**, as well
344 as a significant (~28%) reduction of REMS time mostly in the light phase **(Figures S5D-S5G)**.
345 Moreover, ABC-Slp-S mice displayed significantly less episodes of NREMS, REMS, or wake in
346 the 24-h cycle, but with longer NREMS episode duration than ABC-eGFP mice, indicative of more
347 consolidated NREMS **(Figures S5H-S5J)**. Accordingly, ABC-Slp-S mice also transitioned less
348 frequently between NREMS and REMS, from REMS to wake and from wake to NREMS **(Figure**
349 **S5K)**. By contrast, ABC-Slp-S^{K37M} mice, which expressed a kinase dead Slp-S, exhibited no sleep
350 phenotype as compared to ABC-eGFP mice **(Figures 5D-5F and S5D-S5K)**. Collectively, these
351 results indicate that ABC-expression of Slp-S causes mild hypersomnia in a manner dependent on
352 its kinase activity.
353
354 **Both long and short isoforms of SLP kinase contribute to hypersomnia in *Sik3*$^{Slp/+}$ mice**
355 It was impossible to study the sleep phenotypes caused by ABC-expression of the long
356 isoforms of SLP owning to the packaging size limit of AAV. A highly conserved inhibitory
357 phosphorylation site, serine 551 (S551), was deleted in all SLP isoforms as it was encoded by the
358 skipped exon 13 of *Sik3* gene (Funato et al., 2016). Accordingly, homozygous *Sik3*^{S551A} knockin
359 mice, which contain the S551A phosphor-mutation, exhibit a marked hypersomnia phenotype
360 mimicking that of *Sik3*^{Slp} mice, underscoring the functional significance of S551 phosphorylation
361 (Funato et al., 2016; Honda et al., 2018). Thus, we constructed the *Sik3*$^{S551A\text{-}L}$ knockin mice by

362 replacing the exon 13 sequence of *Sik3* with the C-terminal cDNA sequence of *Sik3-L*, the longest
363 *Sik3* isoform that carried the S551A mutation and was immediately followed by the
364 polyadenylation sequence **(Figures 5G and 5H)**. Immunoblotting of whole brain extracts from
365 homozygous $Sik3^{S551A\text{-}L}$ mice confirmed that this $Sik3^{S551A\text{-}L}$ allele could only encode the $SIK3^{S551A}$-
366 L isoform **(Figure 5I)**.

367 Because homozygous $Sik3^{S551A\text{-}L}$ mice were rarely viable, we compared the sleep
368 phenotypes of wild-type and heterozygous mice by EEG/EMG recording. Relative to wild-type
369 littermates, heterozygous $Sik3^{S551A\text{-}L}$ mice exhibited ~90 min increase in daily NREMS time,
370 accompanied by elevated NREMS delta power mainly in the dark phase **(Figures 5J-5L)**.
371 Additionally, $Sik3^{S551A\text{-}L}$ mice spent less time awake during the dark phase or in REMS during the
372 light phase, with elevated delta power in REMS and increased theta power during wakefulness
373 **(Figures S6A-S6E)**. Furthermore, we performed intravenous injection of AAV-hSyn-Slp-S in
374 heterozygous $Sik3^{S551A\text{-}L}$ mice, in which ABC-expression of Slp-S resulted in a stronger
375 hypersomnia phenotype as shown by compound increases in NREMS amount and delta power as
376 well as corresponding reductions in total REMS and wake time **(Figures 5M-5O and S6F-S6J)**.
377 Taken together, these results suggest that both long and short isoforms of SLP kinases contribute
378 critically to the hypersomnia of $Sik3^{Slp/+}$ mice.

379

380 **ABC-KO of specific genes by triple-target CRISPR in Cas9 mice**

381 We envisioned that it would be more direct and faster to generate ABC-KO mice with the
382 use of CRISPR/Cas9 technology. In this system, Cas9 nuclease is directed by single-guide
383 (sg)RNA to introduce site-specific DNA break in the target gene, which is repaired by the error-
384 prone non-homologous end-joining pathways, resulting in indel mutations (e.g., short deletions or
385 insertions) that may disrupt gene function (Hsu et al., 2014; Jinek et al., 2012; Wang et al., 2013).

386 However, these Cas9-mediated indel mutations occur at a moderate frequency and not all mutations
387 can ablate target gene function.

388 Although it is routine to knockout a target gene by CRISPR/Cas9 *via* local injection of
389 AAV expressing sgRNA into specific brain regions of Cas9 mice, there is no report of systemic
390 ABC-KO of target gene in the adult mouse brain by CRISPR/Cas9 via intravenous injection of
391 AAV expressing sgRNA. A big challenge for ABC-KO by CRISPR/Cas9 is that the vast majority
392 of adult brain neurons are non-dividing, terminally differentiated cells. Thus, the efficiency of KO
393 by CRISPR needs to be nearly perfect, that is, both alleles of target gene are disrupted in almost all
394 AAV-PHP.eB-infected neurons. To improve the efficiency of CRISPR KO, multiplexing strategies
395 using several sgRNAs have been utilized to simultaneously target the same gene in various model
396 organisms (Port et al., 2020; Xie et al., 2015; Yin et al., 2015). A triple-target CRISPR method can
397 produce whole-body biallelic knockout mice with 96-100% efficiency in a single generation
398 (Sunagawa et al., 2016; Tatsuki et al., 2016). Therefore, we decided to try this method to generate
399 ABC-KO mice by retro-orbital injection of Cas9 mice with AAV-PHP.eB expressing three
400 sgRNAs targeting the same gene **(Figure 6A)**.

401 To demonstrate the proof-of-principle for ABC-KO by CRISPR/Cas9, we chose to
402 knockout *NeuN*, a ubiquitously expressed gene in the adult brain neurons, in Cre-dependent Cas9-
403 expressing mice by injection of AAV-PHP.eB expressing HA-Cre recombinase from the hSyn
404 promoter as well as one, two, or three U6:sgRNA cistrons targeting *NeuN* **(Figure 6B)**. We found
405 that the efficiency of ABC-KO of *NeuN* was significantly higher with triple sgRNAs than with
406 single or double sgRNAs **(Figure S7A)**. Moreover, the efficiency of ABC-KO of *NeuN* peaked at
407 three weeks after AAV injection and increased in a viral dose-dependent manner **(Figures S7B and**
408 **S7C)**. Whole genome sequencing of AAV-3xsgRNA^{NeuN} injected mouse brain DNA demonstrated
409 on-target indel mutations and large inter-exon deletions, but rarely off-target mutations **(Figures**
410 **6C and S7D)**. Immunoblotting showed that the level of NeuN expression was specifically reduced

411 by ~70%, whereas another pan-neuronal protein Tublin J remain unchanged in whole brain lysates
412 of AAV-3xsgRNA^{NeuN} injected mice **(Figures 6D and 6E)**. Accordingly, co-immunostaining of
413 NeuN and HA-Cre revealed that expression of NeuN disappeared in the majority of AAV-
414 3xsgRNA^{NeuN}-infected adult brain neurons **(Figure 6F)**.

415 Next, we performed ABC-KO of *Sik3* gene, which was broadly expressed in the adult brain
416 neurons (Funato et al., 2016), by injecting *Sik3*$^{Slp/+}$; *Rosa26*$^{Cas9/+}$ (constitutive Cas9-expressing)
417 adult mice with AAV-PHP.eB expressing three non-target sgRNAs (AAV-sgRNA^{NT}) or one of two
418 sets of three sgRNAs (AAV-sgRNA^{Sik3}) targeting different exons of *Sik3* gene **(Figure S7G)**. Both
419 long and short isoforms of SIK3/SLP proteins were reduced by ～80% in whole brain lysates of
420 both sets of AAV-sgRNA^{Sik3} injected mice relative to AAV-sgRNA^{NT} injected mice **(Figures 6G,**
421 **6H and S7E, S7F)**. Furthermore, we attempted double ABC-KO of histone deacetylases HDAC4
422 and HDAC5 in Cas9 mice by co-injection of two AAV-PHP.eB viruses respectively expressing
423 three sgRNAs targeting the *Hdac4* or *Hdac5* gene **(Figure S7H)**. Immunoblotting indicated that the
424 levels of both HDAC4 and HDAC5 proteins were reduced by ~70-80% in ABC-HDAC4/5^{DKO}
425 brain lysates relative to the control brain lysates **(Figures 6I and 6J)**. It is worth noting that the
426 ~70-80% efficiency of ABC-KO of *NeuN*, *Sik3*, or *Hdac4/5* seemed to be significantly better than
427 the ~40-80% viral transduction rates of adult brain neurons as measured by immunohistochemistry.
428 We speculated that the viral transduction rates could be underestimated by immunostaining of
429 proteins and that low level of sgRNAs expression might be sufficient to KO target genes in the
430 AAV-PHP.eB-infected neurons.

431

432 **ABC-KO of *Slp* allele rescues the hypersomnia of *Sik3*$^{Slp/+}$ mice**

433 We showed that ABC-KO of exon 13 of *Sik3* by AAV-hSyn-Cre injection in *Sik3-E13*$^{flox/flox}$
434 adult mice could induce hypersomnia similar to that of *Sleepy* mice **(Figure 4J-4L)**. Conversely,
435 we hypothesized that ABC-KO of *Slp* should rescue the hypersomnia of *Sik3*$^{Slp/+}$ mice. Indeed,

436 ABC-KO of both *Slp/Sik3* alleles by triple-target CRISPR resulted in ~150 min reduction in daily
437 NREMS time and reduced NREMS delta power in *Sik3*$^{Slp/+}$, *Rosa26*$^{Cas9/+}$ male mice **(Figures 7A-**
438 **7C and S8A-S8E)**. Similarly, ABC-KO of *Slp/Sik3* alleles by CRISPR/Cas9 using a second set of
439 triple sgRNAs caused ~180 min reduction in daily NREMS time and diminished NREMS delta
440 power in *Sik3*$^{Slp/+}$, *Rosa26*$^{Cas9/+}$ female mice **(Figures 7D-7F and S8F-S8J)**. Therefore, the
441 hypersomnia of *Sik3*$^{Slp/+}$ mice is largely reversable by disrupting SLP expression in the adult brain
442 neurons. These results strongly suggest that the hypersomnia phenotype of *Sik3*$^{Slp/+}$ mice requires
443 continuous expression of mutant SLP kinases, which probably constitutively phosphorylate
444 substrate proteins that are critical for the regulation of sleep need (Wang et al., 2018).
445
446 **Double ABC-KO of orexin/hypocretin receptors causes chocolate-induced narcolepsy**
447 **episodes**
448 Previous studies have shown that knockout mice for the neuropeptide orexin/hypocretin or
449 its receptors, OX1R/HCRTR1 and OX2R/HCRTR2 (hereafter OX1R and OX2R for simplicity),
450 exhibit narcolepsy-like phenotypes, such as abnormal wake to REMS transition and cataplexy
451 (Chemelli et al., 1999; Kalogiannis et al., 2010; Kohlmeier et al., 2013). To generate double ABC-
452 KO of OX1R and OX2R, we co-injected Cas9-expressing mice with two AAV-PHP.eB viruses
453 expressing separate sets of triple sgRNAs targeting either *Ox1r* or *Ox2r* gene, respectively. At first,
454 all of the ABC-*Ox1r/Ox2r*^{DKO} mice exhibited no sleep abnormality as compared to the control
455 AAV-sgRNA^{NT} injected mice. Remarkably, after feeding with chocolates–a known stimulant of
456 narcolepsy (Oishi et al., 2013), three out of eight ABC-*Ox1r/Ox2r*^{DKO} mice exhibited frequent
457 narcolepsy-like episodes **(Figure 7G)**, which was characterized by the abnormal transitions from
458 wake to REMS during the EEG/EMG recording **(Figures 7H and 7I)**. However, we did not
459 observe cataplexy during the narcolepsy episodes through coupled video/EEG recording and
460 manual inspection. This partial narcoleptic phenotype is probably due to incomplete knockout of

461 Ox1R and Ox2R in all of the adult brain neurons. Taken together, these results suggest that
462 multiplex ABC-KO by CRISPR/Cas9 can facilitate one-step analysis of the sleep phenotypes of
463 target genes, including essential or redundant genes, in adult mice without genetic crosses.
464

465 **DISCUSSION**

466 Despite of recent advance in understanding of the neural pathways that control executive
467 sleep/wake switching (Liu and Dan, 2019; Saper et al., 2010; Saper et al., 2005; Weber and Dan,
468 2016), the molecular mechanisms of mammalian sleep regulation are largely unknown. It remains
469 unclear which genes constitute the core sleep regulatory pathways in mice, but also where these
470 genes may function in the mouse brain. Although classical germline mouse genetics remains a
471 powerful approach to identify new sleep regulatory genes, it is unwieldy to study the essential
472 genes or redundant pathways that are likely critical for sleep regulation. It is also challenging to
473 conduct large-scale EEG/EMG-based mouse sleep screening owning to lengthy genetic crosses and
474 labor-intensvie surgeries. In this study, we develop a highly efficient ABC-expression/knockout
475 platform and a highly accurate SleepV (video) system for high-throughput somatic genetics
476 analysis of sleep in adult mice. We demonstrated the proof-of-principle for three powerful
477 applications of this platform: 1) ABC-expression facilitates gain-of-function analysis of sleep
478 regulatory genes; 2) ABC-KO by AAV-Cre injection expedites systematic analysis of conditional
479 flox mice for sleep phenotypes; 3) Multiplex ABC-KO by CRISPR/Cas9 enables one-step analysis
480 of redundant sleep genes in adult mice. Taken together, we believe that this ABC-
481 expression/knockout platform should greatly expedite the identification of core sleep regulatory
482 pathways and elucidation of molecular mechanisms of sleep regulation in mammals. Furthermore,
483 we envision that these somatic genetics approaches should facilitate efficient and sophisticated
484 studies of diverse brain-related cellular, physiological and behavioral processes in adult mice by
485 skipping the development and genetic crosses.

486

487 **AAV-Cre injection facilitates systematic sleep screening of conditional flox mice**

488 We showed that intravenous injection of *Creb1*$^{flox/flox}$ adult mice with AAV-hSyn-Cre could
489 efficiently knockout CREB expression in the adult brain neurons, resulting in a significant increase
490 in daily NREMS amount. On the other hand, AAV-hSyn-Cre injection could efficiently excise
491 exon 13 of *Sik3* in the adult brain neurons of *Sik3-E13*$^{flox/flox}$ mice, resulting in a functionally
492 equivalent *Slp* allele and marked hypersomnia mimicking that of *Sik3*$^{Slp/Slp}$ mice. Thus, ABC-KO by
493 Cre/loxP-mediated recombination can create either loss- or gain-of-function somatic mutations of
494 target gene in the adult brain neurons, resulting in strong sleep phenotypes in adult mice. A
495 significant recent development for mouse genetics community is the development of a large
496 repertoire of conditional flox strains for most if not all of mouse genes from the International
497 Knockout Mouse Consortium (IKMC) as well as commercial sources. Therefore, we envision that
498 ABC-KO by AAV-delivered Cre expression from ubiquitous or cell type-specific promoters, such
499 as the hSyn (neurons), CaMKII (excitatory neurons), or GFAP (astrocytes) promoters, represents
500 an efficient method for systematic screening of conditional flox mice for sleep and other
501 phenotypes.

502

503 **How to distinguish primary vs. secondary sleep phenotypes?**

504 Because a large number of genes play important roles in the development of mouse brain, it
505 is often uncertain whether the sleep phenotype of a mutant mouse strain is the primary phenotype
506 or secondary phenotype resulting from developmental abnormalities of the brain. Alternatively, it
507 is also possible that the sleep phenotype could be indirectly attributed to the dysfunctions of
508 peripheral organs rather than the brain. The ABC-expression/knockout platform can be used to
509 effectively address this challenging question by skipping the development altogether and directly
510 assessing the sleep phenotype of somatic mutations in the adult brain cells. For example, ABC-KO

511 of exon 13 of *Sik3* by AAV-mediated Cre/loxP recombination in the adult brain neurons induced
512 hypersomnia in *Sik3-E13*$^{flox/flox}$ mice, whereas ABC-KO of *Slp* allele by CRISPR/Cas9 largely
513 reversed the hypersomnia of *Sik3*$^{Slp/+}$ mice. These results strongly suggest that the hypersomnia of
514 *Sleepy* (*Sik3*^{Slp}) mutant mice is the primary phenotype resulting from the direct effects of mutant
515 SLP kinases on the sleep regulatory apparatus in the adult brain neurons. Thus, this type of somatic
516 genetics analysis can serve as a powerful tool to distinguish between the primary and secondary
517 sleep phenotypes for candidate genes that are also important for brain development or peripheral
518 tissue functions.
519

520 **Multiplex ABC-KO by CRISPR enables one-step analysis of redundant sleep genes**

521 To analyze the sleep phenotypes of redundant genes, it is both costly and time-consuming
522 (≥ 2 years) to generate double or triple knockout mice through classical germline genetics
523 approaches (Sunagawa et al., 2016). Although a combination of triple-target CRISPR and modified
524 embryonic stem cell technologies allows for biallelic knockout of multiple genes in a single
525 generation, this strategy only works for non-essential genes (Sunagawa et al., 2016). Here, we
526 successfully generated ABC-KO mice by triple-target CRISPR *via* intravenous injection of Cas9
527 mice with AAV-PHP.eB expressing three sgRNAs targeting one gene. It was estimated that this
528 method achieved efficient biallelic knockout of *Sik3/Slp* in ~80% of the adult brain neurons, which
529 could largely rescue the hypersomnia phenotype of *Sik3*$^{Slp/+}$ mice. Furthermore, double ABC-KO of
530 OX1R and OX2R in adult Cas9 mice resulted in chocolate-induced narcolepsy episodes. It should
531 be noted, however, that the efficiency of multiplex ABC-KO by CRISPR/Cas9 may not be optimal
532 in all cases, which can be further improved by optimizing the sgRNA structure or pre-screening of
533 individual sgRNAs and potentially by developing other CRISPR/Cas systems. For example, unlike
534 CRISPR/Cas9 that requires three U6:sgRNA cistrons to target one gene, the CRISPR/Cpf1 (Cas12a)
535 and CRISPR/Cas13d (targeting RNA) systems can process a polycistronic transcript into multiple

536 gRNAs targeting the same or different genes (Konermann et al., 2018; Zetsche et al., 2017; Zhong
537 et al., 2017). Therefore, we believe that multiplex ABC-KO by CRISPR/Cas will greatly expedite
538 one-step analysis of redundant sleep genes in adult mice without genetic crosses, which can be
539 achieved in less than 2 months and is applicable for both essential and non-essential genes.
540

541 **Rapid, efficient and sophisticated somatic genetics analysis**

542 Mosaic genetic analysis–the study of phenotypes resulting from homozygous mutant cells
543 in a heterozygous background–has been widely used to study tissue-specific functions of genes in
544 the worms, flies and zebrafish (Carmany-Rampey and Moens, 2006; Xu and Rubin, 1993; Yochem
545 and Herman, 2003). Moreover, high frequency of generating mosaic animals by the Flp/FRT-
546 mediated site-specific recombination makes it possible to conduct mosaic genetic screens in the
547 fruit flies, which have made seminal contributions to a variety of fields, including development,
548 stem cells, cell competition, apoptosis, and cancer (de la Cova et al., 2004; Harvey et al., 2003;
549 Huang et al., 1999; Lee and Luo, 1999; Li and Baker, 2007; Moreno and Basler, 2004; Pagliarini
550 and Xu, 2003; Potter et al., 2001; Xie and Spradling, 1998; Xu et al., 1995). Similar mosaic
551 strategies, such as MADM (mosaic animals with double marker) and MASTR (mosaic mutant
552 animals with spatial and temporal control of recombination), have been developed in mice (Lao et
553 al., 2012; Muzumdar et al., 2007; Wang et al., 2007; Zong et al., 2005). However, such mosaic
554 genetic analysis are difficult to conduct in mice and have limited scope of biological applications
555 because of complicated genetic crosses (3 months per generation) and low efficiency of mitotic
556 recombination.

557 The AAV-based ABC-expression/knockout platform represents an innovative approach to
558 conduct rapid, efficient and sophisticated somatic mosaic experiments in mice. For example, when
559 ABC-expression/KO of two target genes produce different or opposite sleep phenotypes, classical
560 epistasis analysis can be easily conducted to determine whether the two genes operate in the same

561 or parallel pathways and map the order of these genes if they are in the same pathway. For in-depth
562 structural and functional analysis of key sleep regulators, ABC-expression of wild-type and mutant
563 proteins can be conducted to rescue the sleep phenotypes of ABC-KO mice for the endogenous
564 proteins. Furthermore, we can efficiently carry out a suppressor screen to identify the downstream
565 effectors of SLP/SIK3 kinases in sleep regulation by ABC-expression of candidate proteins in
566 *Sleepy* (*Sik3*$^{Slp/+}$) mice, or by ABC-KO of target genes in *Sik3*$^{Slp/+}$, *Rosa26*$^{Cas9/+}$ mice. Conversely,
567 the ABC-expression/knockout platform can also be used for enhancer screens to uncover redundant
568 sleep genes or pathways. These sophisticated somatic genetic analyses of sleep genes in adult mice
569 can be rapidly and efficiently performed without the need for time-consuming construction and
570 complicated genetic cross of germline mutant mice.

571 Classical forward and reverse mouse genetics have contributed enormously to our
572 understanding of the molecular mechanisms of human physiologies and diseases (Moresco et al.,
573 2013; Takahashi et al., 1994). We believe that this ABC-expression/knockout platform could be
574 broadly applied for somatic genetics screening of mouse genes in other brain-related processes,
575 such as circadian clock, learning and memory, innate and learned fear, brain injury/repair and
576 cancer. Moreover, similar strategies can be developed to facilitate studies of tissue-specific
577 functions of mouse genes using AAV variants engineered to efficiently transduce other peripheral
578 organs besides liver, such as the heart, kidney, muscle, lung, skin, testis and ovary (Chan et al.,
579 2017; Gradinaru, 2020; Pulicherla et al., 2011). Finally, the ABC-expression/knockout platform has
580 great potential for development of novel gene therapies for human diseases, including various
581 neurodegenerative disorders (Borel et al., 2014; Hocquemiller et al., 2016; Kaplitt et al., 2007;
582 Marchio et al., 2016; Ojala et al., 2015; Wu et al., 2006).

583

584

585

586 **ACKNOWLEDGEMENTS**

587 We are thankful for Drs. M. Luo and F. Shao for sharing reagents; K. Wu, Z. Li, W. Min, Y.
588 Zhuang, H. Huang, and Y. Yin for technical assistance; Drs. X. Wang, F. Shao, R. Xi, and N. Tang
589 for discussion and comments on the manuscript; M. Shi for graphical abstract design. This work
590 was supported by the Natural Science Foundation of China (61772526 to Z.C.), the Beijing
591 Municipal Science and Technology Commission (Z181100001318004 to Q.L.) and the National
592 Key Research and Development Program of China.

593

594 **AUTHOR CONTRIBUTIONS**

595 Q.L., G.W., Q.L., J.X., S.Z., R.Z. designed and executed the experiments with help from F.W.,
596 Z.C.; G.W. Q.L., J.X., R.Z. developed the ABC-expression/KO platform and performed molecular
597 genetics experiments with help from Z.C., W.J.; S.Z., Q.L., Z.C. developed the SleepV (video)
598 system; X.G., S.Z., Z.C., C.M., L.C., B.S. performed EEG/EMG recording and analysis; F.W., R.Z.
599 generated multiple mouse strains; Q.S., Y.G. performed AAV packaging and purification; H.W.,
600 X.W., H.L. helped mouse husbandry. G.W., Q.L., J.X., S.Z., R.Z.prepared the figures and Q.L.,
601 wrote the manuscript with help from G.W., Q.L.

602

603 **Data availability**

604 All raw data in this study are available from the corresponding authors upon reasonable request.

605

606 **Competing interests**

607 We declare no competing interests.

608

609 **METHODS**

610 **Animals**

611 All animal experiments were performed according to procedures approved by the
612 institutional Animal Care and Use Committee of National Institute of Biological Sciences, Beijing
613 (NIBS). All mice were provided food and water *ad libitum* and were housed under humidity and
614 temperature controlled conditions (22-24°C) on a 12 light: 12h dark cycle. *Rosa26-Cas9* (JAX
615 026179) and *Rosa26-LSL-Cas9* (JAX 026175) were purchased from the Jackson laboratory.
616 *Creb1*^{flox} mice were generated by flanking exon4 of *creb1* with two loxP sites. *Sik3-E13*^{flox} mice
617 were constructed by flanking exon13 of *sik3* with two loxP sites. *Sik3*$^{S551A\text{-}L}$ mice were generated by
618 mutating S551A and inserting Sik3 long isoform (544-1369aa) and bGH poly(A) in the exon13 of
619 *Sik3* at the nucleotide position of 185839. These flox and knock-in mice were generated by
620 CRISPR/Cas9 in the transgenic animal facility at NIBS.

621

622 **DNA Constructs**

623 AAV: EF1α-DIO-H2B-eGFP plasmid was a gift from Dr. Minmin Luo's lab (NIBS).
624 pAAV-CBh-Cre was constructed by subcloning the CBh-Cre cassette from AAV:ITR-U6-
625 sgRNA(backbone)-CBh-Cre-WPRE-hGHpA-ITR (Addgene, 60229) into pAAV-hSyn-eGFP
626 (Addgene, 105539). pAAV-hSyn-Cre was modified from pAAV-hSyn-eGFP (Addgene, 105539)
627 by replacing eGFP with Cre. pX600-hSyn vector was modified from pX600-AAV-CMV::NLS-
628 SaCas9-NLS-3xHA-bGHpA (Addgene, 61592) by replacing CMV promoter with hSyn promoter.
629 The sgRNA sequences were designed based on Mouse GeCKO v2 Library and database from
630 RIKEN (Sanjana et al., 2014; Sunagawa et al., 2016). Annealed oligos for sgRNAs were firstly
631 inserted into the AAV-ITR-U6-sgRNA(backbone)-hSyn-Cre-2A-EGFP-KASH-WPRE-shortPA-
632 ITR (Addgene, 60229) vector. Then, the pAAV plasmids contain double or triple U6:sgRNA
633 cistrons were constructed through PCR amplification, restriction digestion and ligation.

634

635 ***Sik3-S* identification**

636 RNAs were extracted from *Sik3*$^{+/+}$, *Sik3*$^{Slp/+}$, *Sik3*$^{Slp/Slp}$ mice and the cDNAs were obtained
637 thorough Reverse Transcription-Polymerase Chain Reaction (RT-PCR) by FastKing one step RT-
638 PCR Kit (TIANGEN, KR116). We designed forward (F: ATGGCCGCTCGCATCGGCTA) primer
639 from N-terminal 59aa of *Sik3* and reverse (R: AGCACTGCCAGGTGCCAC) primer in the 3' UTR
640 of *Sik3-S* for *Sik3/Slp-S* identification. *Sik3/Slp-S* PCR products were purified by gel extraction kit
641 (Biomed, DH101) as template for second round PCR for *Sik3-S* N-terminal sequencing. (F:
642 ATGGCCGCTCGCATCGGCTA; R: CCCGCAGATTCTGCAGTG TGC). Slp-S and Slp-S^{K37M}
643 were then cloned into the pX600-hSyn vector.

644

645 **AAV-PHP.eB packaging and purification**

646 AAV-PHP.eBs were packaged in AAVpro 293T cells (Clontech, 632273). Cells were
647 harvested by cell lifter (Biologix, 70-2180) 72 h after co-transfection with PHP.eB (Addgene,
648 103005), pHelper (Agilent, 240071-54) and transfer plasmids using polyethylenimine MAX
649 (Polysciences, 24765). The cell pellets were suspended in 1X Gradient Buffer (10mM Tris-HCl
650 pH=7.6, 150mM NaCl, 10mM $MgCl_2$). Cells were lysed by five repeated cycles of liquid nitrogen
651 freezing, 37°C water bath thawing and vortex. Then the cell lysate was mixed with ≥50 U/mL of
652 Benzonase nuclease (Milipore, E1014) and incubated at 37°C for 30 min. Centrifuge the cell lysate
653 at 21,130g for 30 min at 4°C and transfer the supernatant to a pre-build iodixanol (Optiprep, D1556)
654 step gradients (15%, 25%, 40% and 58%) for ultracentrifugation purification. Vacuum centrifuge at
655 41000rpm, 4°C for 4 h, the virus particles were in the layer of 40% iodixanol gradient. Accurately
656 insert the needle ~1-2 mm below the interface between the 40% and 58% gradient and extract all
657 the 40% virus containing layer. Purified AAV-PHP.eB were concentrated using Amicon filters
658 (EMD, UFC801096) and formulated in sterile phosphate-buffered saline (PBS) supplemented with

659 0.01% Pluronic F68 (Gibco, 24040032). Virus titers were determined by qPCR using a linearized
660 AAV plasmid as a standard.
661
662 **Tet-on inducible system**
663 The pAAV-Tre-eGFP, pAAV-Tre-CREB^{VP16} and pAAV-Tre-CRTC1^{CA} were constructed
664 by subcloing Tre promoter to pAAV-hSyn-vector. Reverse tetracycline-controlled transactivator
665 (rtTA) expression was driven by the EF1α promoter. Tre promoter and rtTA sequences were
666 obtained from Dr. Feng Shao's lab (NIBS). For Tet-on inducible sleep recording, EEG/EMG
667 surgeries were carried out on 12-weeks old mice. The mice were recovered for one week and AAV-
668 Tre-eGFP, AAV-Tre-CREB^{VP16} or AAV-Tre-CRTC1^{CA} was co-injected with AAV-EF1α-rtTA
669 through retro-orbital injection. After two weeks virus expression, baseline sleep recording was
670 performed for 3 days without Doxycycline. Then the water was changed with 2mg/mL
671 Doxycycline containing water and subjected to EEG/EMG recording for another 3 days.
672
673 **Genomic DNA Extraction and Captured Illumina Sequencing**
674 Genomic DNA was extracted from mouse brain using TIANamp Genomic DNA Kit
675 (TIANGEN, DP304) following the recommended protocol. Genomic DNA (1-1.5 g) was sheared to
676 300 to 400-bp by Covaris S220 (Covaris, Woburn, MA, USA) and purified with 1X magnetic
677 beads (Ampure XP; Beckman Coulter). Sheared DNA fragments was Subjected to Illumina paired-
678 end DNA library using NEBNext ultra II DNA Library Prep Kit (E7645L, NEB).
679 Preparation and PCR-amplified for three cycles and libraries size were selected with 0.55-1X
680 magnetic beads (Ampure XP, Beckman). Amplified libraries were sequenced using the HiSeq X
681 ten Platform (Illumina) as paired-end 150 base reads according to the manufacturer's protocol.
682 Illumina raw sequencing reads were processed through a standard pipeline consisting of
683 low-quality read filtering through Trimmomatic (version 0.36), alignment to mouse genome

684 GRCm38 (mm10) using the Burrows–Wheeler Aligner (BWA, version 0.7.17-r1188) algorithm.
685 The aligned BAM files were processed using the Genome Analysis Toolkit (GATK, version 4.1.4),
686 including mark PCR duplicates and correction for realignments and mapping quality score
687 recalibrations. Haplotype Caller was used for variant calling.

688 Twenty-one potential off-target sites for the three sgRNAs targeting *NeuN* genes listed
689 below were identified using Cas-OFFinder (http://www.rgenome.net/cas-offinder/).

690 NeuN sgRNA-1(TCGGGGTCCCTGAACCGGAAGGG):

691 1. TCtGGaTCCCgGAACCGGAAAGG chr16 7277126 - 3

692 2. TCGGGGTCCCTGAACCactAAGG chr7 30375662 - 3

693 3. TaGGGGTCCCTGAAaCaGAATGG chr7 45640152 - 3

694 4. TgGGGtTCCCTGAACCccAAAGG chrX 11971373 - 4

695 5. TCGGGGTCCCTGAACCacTAAGGG chr7 30375661 - 2

696 6. TCGGGGTCCCTGAACCActAAGGG chr7 30375661 - 2

697 7. TCGGGGTCCCTGAACCaCtAAGGG chr7 30375661 - 2

698 NeuN sgRNA-2(GCTCAGATGCTGACCGAGCCCGG):

699 8. GCTCAGATGCTGACaGAcCtGGG chr16 25376832 + 3

700 9. GCTgAGATGCaGACtGAGCCTGG chr16 30614345 - 3

701 10. GCTCAGcTGCTGgCCcAGCCTGG chr15 82930003 - 3

702 11. GCTtAGATGCTGAtgGAGCCTGG chr7 101383685 + 3

703 12. GCTCAGATGCTGgCCTGtGCCAGG chr9 120120623 + 2

704 13. GCTCAGATGtTGtCCAGAGCCAGG chr5 66096471 - 2

705 14. GCTCAGGcTGCTGACaGAGCtGGG chrX 11232414 + 3

706 NeuN sgRNA-3(GCTGAATGGGACGATCGTAGAGG):

707 15. GCTGttTGGGAgGATCGTAGAGG chr13 48330995 + 3

708 16. GCTGtATGGtAgGATCGTAGGGG chr4 22110214 + 3

709 17. GCTGAATGGGAgGATCaTcaGGG chrX 98480354 - 4

710 18. GCTGAATGGagCGATgGgAGAGG chr15 10917958 - 4

711 19. GCTGGAATGtGAgGATaGTAGTGG chrX 164503183 + 3

712 20. GCTGGAATGtGAgGATaGTAGTGG chrX 164503183 + 3

713 21. GCTGgATGGGACGATgGTACtTGG chr8 28174078 + 3

714

715 **EEG/EMG surgery**

716 All EEG/EMG surgeries were performed by experienced technicians. 11 to 13-weeks old
717 male or female mice (all experiments were conducted with male mice if not indicated otherwise)
718 were anesthetized by isoflurane (4% for induction, 2% for maintenance) and surgical tools were
719 sterilized by ethanol just before use. After confirming the mice lack of pain, the head region was
720 shaved, cleaned with ethanol and the skull was exposed. The exposed skull was cleaned by cotton
721 swabs to improve binding of skull and dental cement. Handheld electrical drill was moved to the
722 lambda point and set the coordinate as (0, 0, 0). Then four holes were drilled by the electrical drill
723 in the skull. The coordinate of the holes were (-1.27, 0, 0), (-1.27, 5.03, 0), (1.27, -5.03, 0) and
724 (1.27, 0, 0). Then the EEG electrode pins were implanted to the dura under stereotaxic control and
725 the EMG wires were inserted into the neck muscle and then stick to the skull with dental cement.
726 After surgery, the mice were housed individually to recover for one week. Then retro-orbital
727 injection of AAV-PHP.eB was performed. After allowing time for virus expression (1 week for
728 ABC expression and 2 weeks for ABC-KO), the mice were tethered to a counterbalanced arm
729 (Instech Laboratories) that allowed free movement and exerted minimal weight for one week
730 before EEG/EMG recording.

731

732 **EEG/EMG recording and data analysis**

733 Three days of baseline EEG/EMG recording were conducted after mice were acclimated for
734 one week recording condition. The sleep–wake behaviors were analyzed as previously described
735 with modifications (Funato et al., 2016). EEG/EMG data were visualized and analyzed using a
736 custom semi-automated staging MatLab (MathWorks)-based program, followed by visual
737 inspection. Following semi-automated analysis of EEG/EMG data, EEG signals were subjected to
738 fast Fourier transform analysis for 1 to 30Hz with 1-Hz bins. Sleep/wake state was staged into
739 NREMS, REMS and wake. NREMS was staged by high amplitude, delta (1–4 Hz) frequency EEG
740 and low EMG tonus. REMS was characterized based on theta (6–9Hz)-dominant EEG and EMG
741 muscle atonia. Wake was staged based on the presence of low amplitude, fast EEG and high
742 amplitude, variable EMG signal. For the NREMS delta power density analysis, hourly averages of
743 delta density were defined by the ratio of delta power (1–4 Hz) to total power of NREMS EEG. For
744 the power spectrum analysis of NREMS, REMS and wake, the EEG power of each frequency bins
745 was expressed as the percentage of total EEG power over all frequency bins (1–30 Hz) in each state.
746

747 **Brain lysate preparation and Immunoblotting**

748 Mouse brains were quickly dissected and flash frozen in liquid nitrogen. Brain tissues were
749 homogenized using mortar/pestle with liquid nitrogen and then lysed in ice-cold RIPA buffer
750 (50mM Tris-HCL pH=7.4, 150mM NaCl, 1% Triton X-100, 0.1% SDS) (Beyotime, P0013B)
751 freshly supplemented with protease and phosphatase inhibitor cocktail tablets (Roche) for 30 min
752 and centrifuged at 21,130g for 15 min at 4°C. The supernatant was transferred to a new tube and
753 boiled at 95°C for 10 min with SDS-loading buffer. Western blotting was performed according to
754 standard protocols using the following antibodies. Rabbit polyclonal anti-SIK3 antibodies were
755 generated using Abcam custom antibody production service. The following antibodies were
756 purchased from commercial sources: anti-CREB (CST, 9197S), anti-NeuN (Milipore, ABN78),
757 anti-HDAC4 (Abcam, ab12172), anti-HDAC5 (SCBT, sc-133106), anti-β-ACTIN (Beyotime,

758 AF003), anti-Tublin J (CST, 5568), anti-GFP (Beyotime, AG279), anti-Cas9 (Abcam, ab204448),
759 anti-HA (Sigma, H6533).
760
761 **Immunohistochemistry**
762 Mice were deeply anesthetized by choral hydrate and perfused transcardially with 0.9%
763 normal saline followed by 4% paraformaldehyde in PBS. Brains were post-fixed in 4%
764 paraformaldehyde in PBS at room temperature for at least 4 hours followed by incubation in 30%
765 sucrose in PBS at room temperature for 24 h. The cryo-protected brains were sectioned at 40
766 micron on a cryostat microtome (Leica). After washing in PBST(0.3% Triton X-100 in PBS) for 5
767 min three times, brain sections were incubated in blocking solution (3% BSA, 0.3% Triton X-100
768 in PBS) at room temperature for 1-h. Then brain sections were incubated with the primary
769 antibodies overnight at 4 ℃ and immunofluorescence tagged secondary antibodies at room
770 temperature for 2-h. After staining, the brain sections were mounted on adhesion microscope slides
771 (Genview) and encapsulated in sealed tablets containing 3 mg/mL DAPI (Solarbio, C0060).The
772 following antibodies were used: anti-HA (1:500, Roche, 11867423001), anti-NeuN (1:500,
773 Milipore, ABN78), anti-GFP (1:2000, Abcam, ab13970).
774
775 **Video-based sleep recording and screening**
776 For video-based sleep screening, adult (9-11 weeks) C57BL/6J male mice were retro-
777 orbitally injected with 10^{12} AAV-PHP.eB viruses expressing different cDNAs from the hSyn
778 promoter. The cDNAs of Arc, Homer1a, Rab3a, Plk2-dn (332-682aa), CamKIIα, CamKIIβ,
779 CaMKIV-dn (K75E), CDK5, CREB and CRTC1 were cloned from mouse brain cDNA library.
780 MEF-VP16 was constructed by fusing MEF2C (1-117aa) with C-terminal VP16-3xHA tag by
781 Gibson assembly. All cDNAs were inserted into pAAV-hSyn-eGFP (Addgene; 105539) by
782 replacing eGFP with individual cDNA. Two weeks after virus injection, mice were individually

783 housed in Ancare cages with food and water provided ad libitum on a 12-h light-12-h dark cycle.
784 The sleep/wake behaviors of the mice were recorded by an infrared camera (704 x 576 resolution)
785 at 25 frames/s. Infrared LED lights were placed above the cages to clearly videotape mouse
786 behaviors in the dark phase. For all sleep recording experiments, 3 days of video data were
787 recorded to calculate the average daily sleep time for each mouse.
788
789 **Automatic sleep staging (SleepV) software for video analysis**
790 The automatic sleep staging of video data consists of two stages: 1) a dedicated video
791 analysis method was developed to extract the mouse information from each sampled frame,
792 including its position coordinates, color, predict and IoU. 2) the mouse state (active or inactive) at
793 the video clip level was obtained by grouping the frame-level information within a time window.
794 (1) Video analysis stage:
795 The suspected regions of interest (ROIs) are first extracted from each sample frame using
796 traditional image processing techniques, such as Gaussian filtering, adaptive and global threshold.
797 More than one ROIs are allowed to be detected because of the complication of food, water gel and
798 shadows caused by environmental light. This multi-detection strategy ensures that the true mouse
799 region is not missed. A deep neural network is used to make a binary classification of each ROI as
800 a mouse or not. This network has been pre-trained on thousands of mouse-no mouse ROI pictures.
801 The ROI with the highest confidence score is designated as the mouse region, while the others were
802 classified as the background noise. According to the ROI size and position coordinate, we extracted
803 several descriptive features, i.e., the network prediction score (predict), the detected mouse mask
804 area (IoU) and the gray information (color) within the detected mask. Similarly, the frame-level
805 features within a time window centered on that frame were also extracted. Denote F_{t} the current
806 frame, {F{t-m}, F{t-m+1}, ... F{t+m}} the frames within this time window, where m is a
807 hyperparameter. The differences between F_{t} and F{t+i}, including predict score difference P_i

808 (predict), mask difference M_i (IoU) and gray pixel difference G_i (color), were calculated and
809 normalized. Then the normalized values were fused to derive a combined score and a threshold was
810 set to derive a preliminary judgment of whether the mouse was active or inactive at frame t.
811 (2) Sleep/wake state determination stage:
812 According to the frame-level preliminary judgment, SleepV defines the sleep state as ≥ 40-s
813 of continuous immobility. To correct misjudgment of subtle movements during sleep, less than 15-s
814 of movement in between two sleep states is also annotated as sleep.
815
816 **Statistical analysis**
817 Statistical analysis of EEG/EMG data was performed using GraphPad Prism 8.0.2.
818 Knockout efficiency measured by Western blot was quantified using ImageJ software. Student's t-
819 test was used for pairwise comparisons, one-way ANOVA for multiple comparisons and two-way
820 ANOVA for multiple comparisons involving two independent variables. Tukey's test compares
821 every mean with every other mean, Dunnett's test compares every mean to a control mean. $p < 0.05$
822 was considered statistically significant.
823

FIGURES

Figure 1. Setup of a video based high-throughput ABC sleep screening platform.

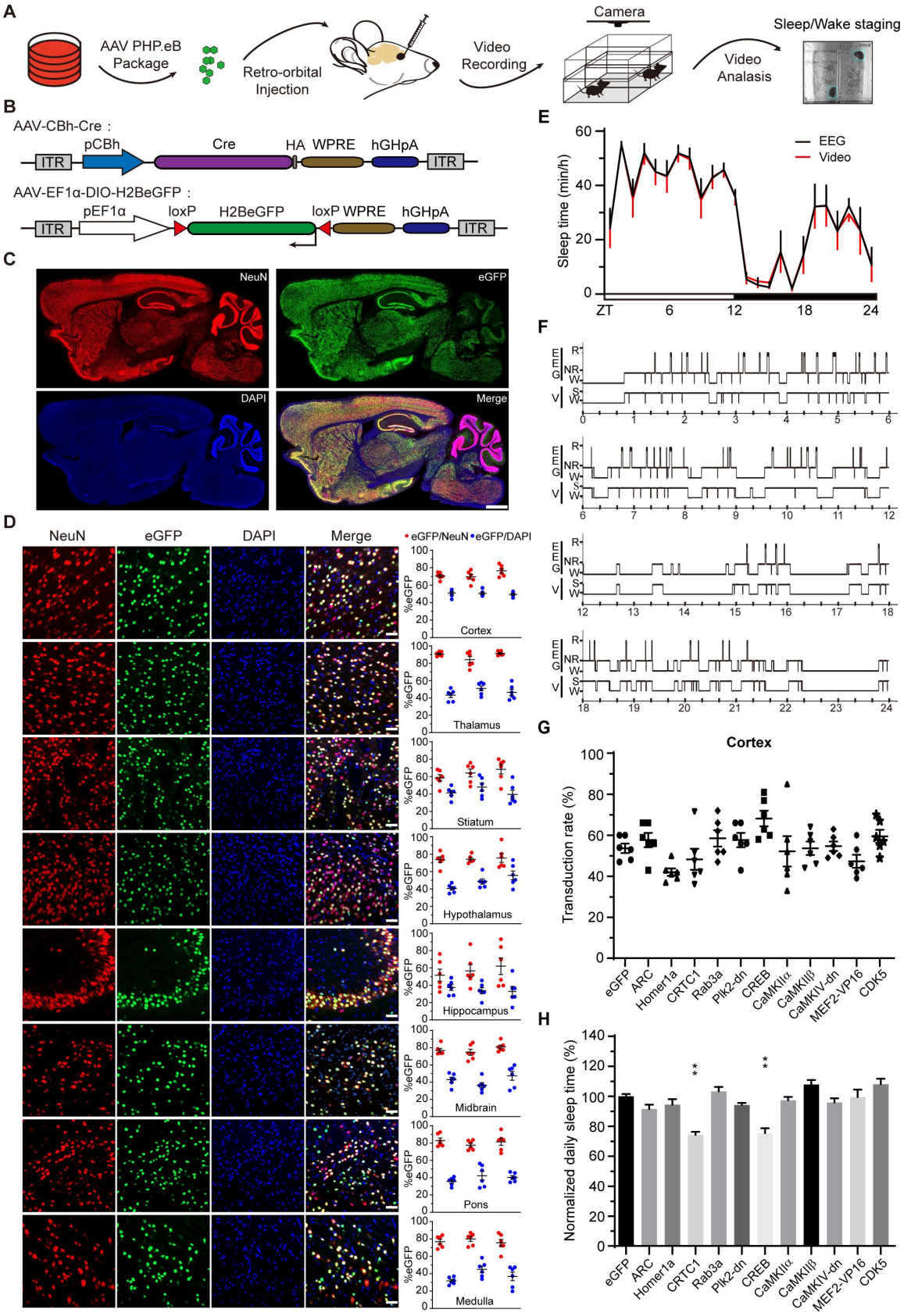

826 **Figure 1. Setup of a video-based high-throughput ABC sleep screening platform.**

827 **(A)** Schematic of the video-based ABC-expression sleep screening platform.

828 **(B)** Schematic of the AAV-CBh:Cre and AAV-pEF1α:DIO-H2B-eGFP constructs.

829 **(C)** Representative images showing co-immunostaining of GFP and NeuN in the sagittal brain

830 sections of AAV-CBh-Cre and AAV-EF1α-DIO-eGFP co-injected mice.

831 **(D)** Representative images and quantification of the percentage of $NeuN^+$ (red) neurons or $DAPI^+$

832 (blue) cells that also express GFP in eight different brain regions.

833 **(E)** Hourly plot of sleep time of six C57BL/6J mice by simultaneous video (red) and EEG/EMG

834 (black) analysis.

835 **(F)** Epoch-by-epoch comparison of sleep/wake staging of the same mouse by simultaneous video

836 (V) and EEG/EMG analysis.

837 **(G)** A graph showing viral transduction rates of cortical neurons in AAV-hSyn-GeneX injected

838 mice expressing different synaptic plasticity regulators from the hSyn promoter.

839 **(H)** A graph showing daily sleep time of ABC-GeneX mice ($n \geq 5$) normalized to that of ABC-

840 eGFP mice.

841 Data are mean ± s.e.m. (H) One-way ANOVA with Dunn's test; ** $p < 0.01$.

842

843

844

Figure 2. ABC-expression of CREB and/or CRTC1 reduces NREMS amount and delta power.

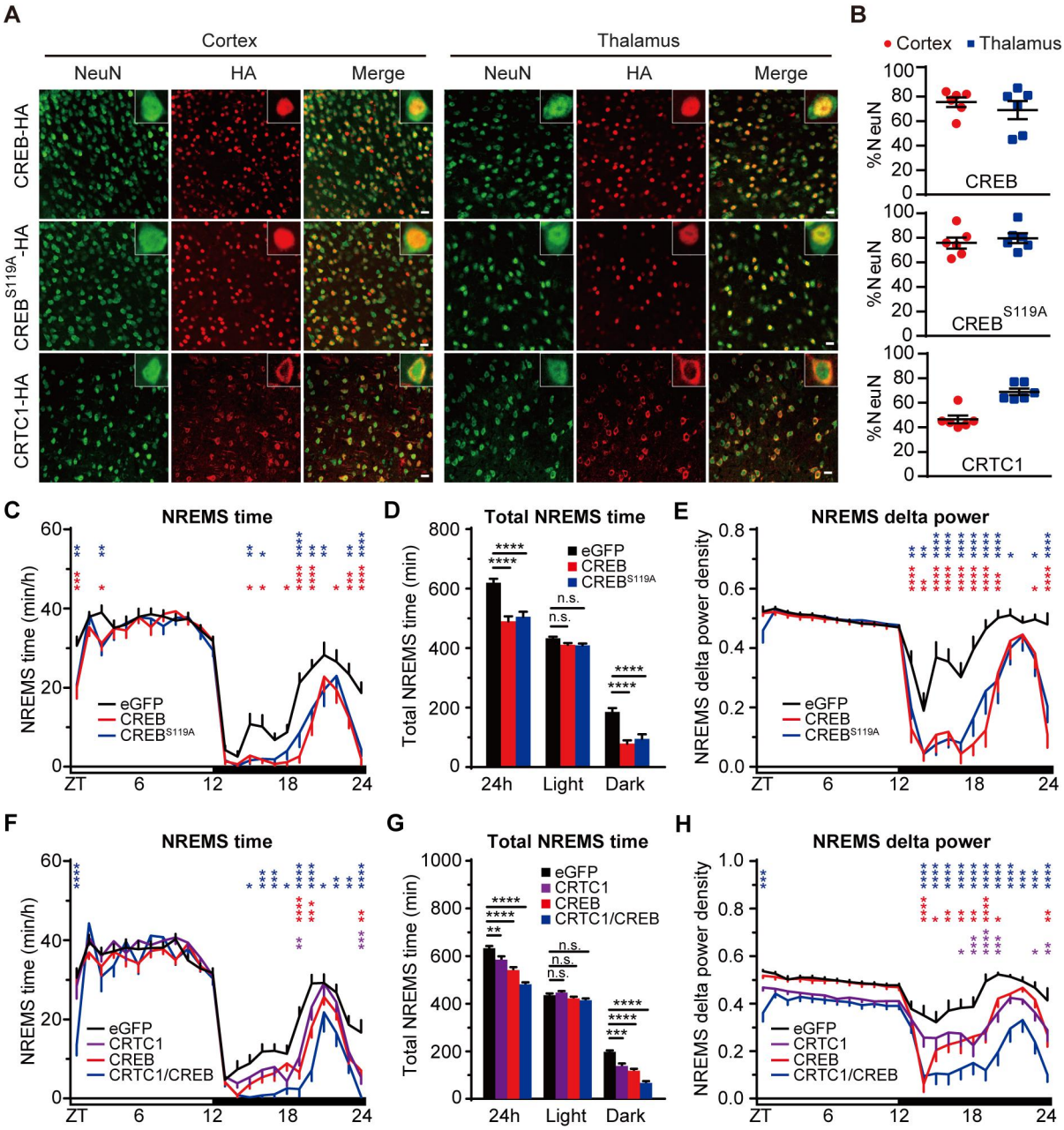

845

846

847

848

849

850

851

852 **Figure 2. ABC-expression of CREB and/or CRTC1 reduces NREMS amount and delta power.**

853 **(A)** Co-immunostaining of HA^+ (red) and $NeuN^+$ (green) neurons in the cortex and thalamus of
854 AAV-hSyn-CREB (ABC-CREB), AAV-hSyn-CREB (ABC-$CREB^{S119A}$) and AAV-hSyn-
855 CRTC1 (ABC-CRTC1)-injected mice.

856 **(B)** Quantification of the viral transduction rates, which is calculated by the percentage of $NeuN^+$
857 neurons that express HA-tagged proteins, in the cortical and thalamic neurons of ABC-CREB,
858 ABC-$CREB^{S119A}$ and ABC-CRTC1 mice.

859 **(C-E)** Hourly plot of NREMS time (C), quantification of total NREMS time (D) and hourly plot
860 of NREMS delta power (E) in the ABC-eGFP (n=11), ABC-CREB (n=12) and ABC-
861 $CREB^{S119A}$ (n=11) mice. Shown above are the statistical analysis for comparison between
862 ABC-CREB (red*) or ABC-$CREB^{S119A}$ (blue*) mice and control ABC-eGFP mice.

863 **(F-H)** Hourly plot of NREMS time (F), quantification of total NREMS time (G) and hourly plot of
864 NREMS delta power (H) in the ABC-eGFP, (n=12), ABC-CRTC1 (n=15), ABC-CREB (n=15)
865 and ABC-CRTC1/CREB (n=12) mice. Shown above are statistical analysis for comparison
866 between ABC-CRTC1 (purple*), ABC-CREB (red*), or ABC-CRTC1/CREB (blue*) mice and
867 control ABC-eGFP mice.

868 Data are mean ± s.e.m. (C-H) Two-way ANOVA with Tukey's test. n.s. not significant; * $p < 0.05$;
869 ** $p < 0.01$; *** $p < 0.001$; **** $p < 0.0001$.

870

Figure 3. Inducible ABC-expression of CREB^{VP16} or CRTC1^{CA} causes significant sleep phenotypes.

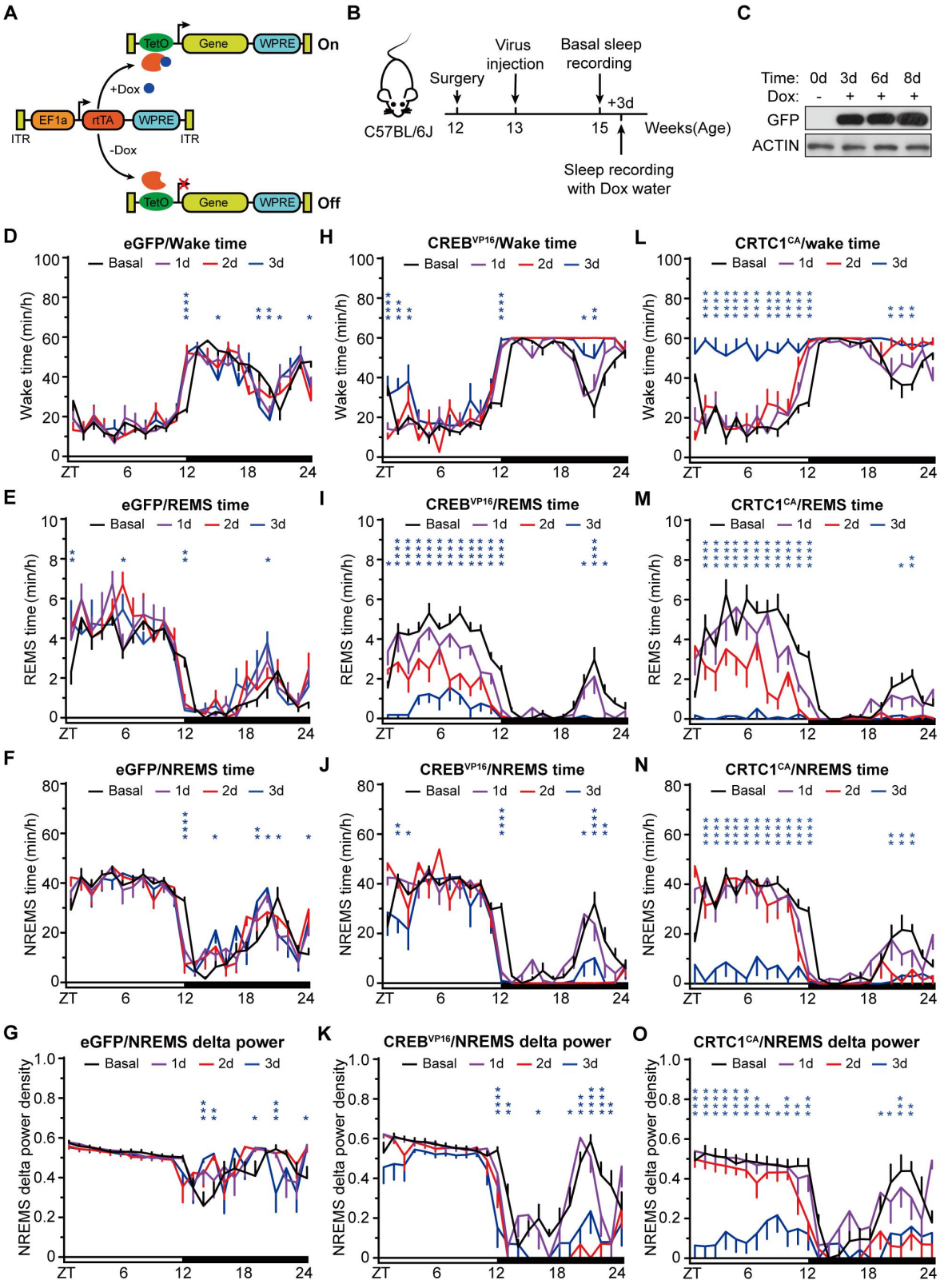

871

872 **Figure 3. Inducible ABC-expression of CREB^{VP16} or CRTC1^{CA} causes significant sleep**
873 **phenotypes.**
874 **(A)** Schematic of Tet-on inducible (i)ABC-expression system with or without Doxcycline (Dox).
875 **(B)** A flow chart of the iABC-expression and EEG/EMG sleep recording experiment.
876 **(C)** Immunoblotting of whole brain lysates from iABC-eGFP mice before and after Dox treatment
877 with anti-GFP and anti-ACTIN antibodies.
878 **(D-G)** Hourly plots of wake time (D), REMS time (E), NREMS time (F) and NREMS delta power
879 (G) of the iABC-eGFP mice (n=8).
880 **(H-K)** Hourly plots of wake time (H), REMS time (I), NREMS time (J) and NREMS delta power
881 (K) in the iABC-CREB^{VP16} mice (n=7).
882 **(L-O)** Hourly plots of wake time (L), REMS time (M), NREMS time (N) and NREMS delta power
883 (O) in the iABC-CRTC1^{CA} mice (n=7).
884 Data are mean ± s.e.m. (D-O) Shown above are statistical analysis for comparison between basal
885 and day 3 (3d) sleep/wake data after Dox treatment. Two-way ANOVA with Tukey's test. * p
886 < 0.05; ** $p < 0.01$; *** $p < 0.001$; **** $p < 0.0001$.
887
888
889
890
891
892
893
894
895

Figure 4. ABC-KO of *Creb1* or exon 13 of *Sik3* by Cre-loxP recombination causes hypersomnia.

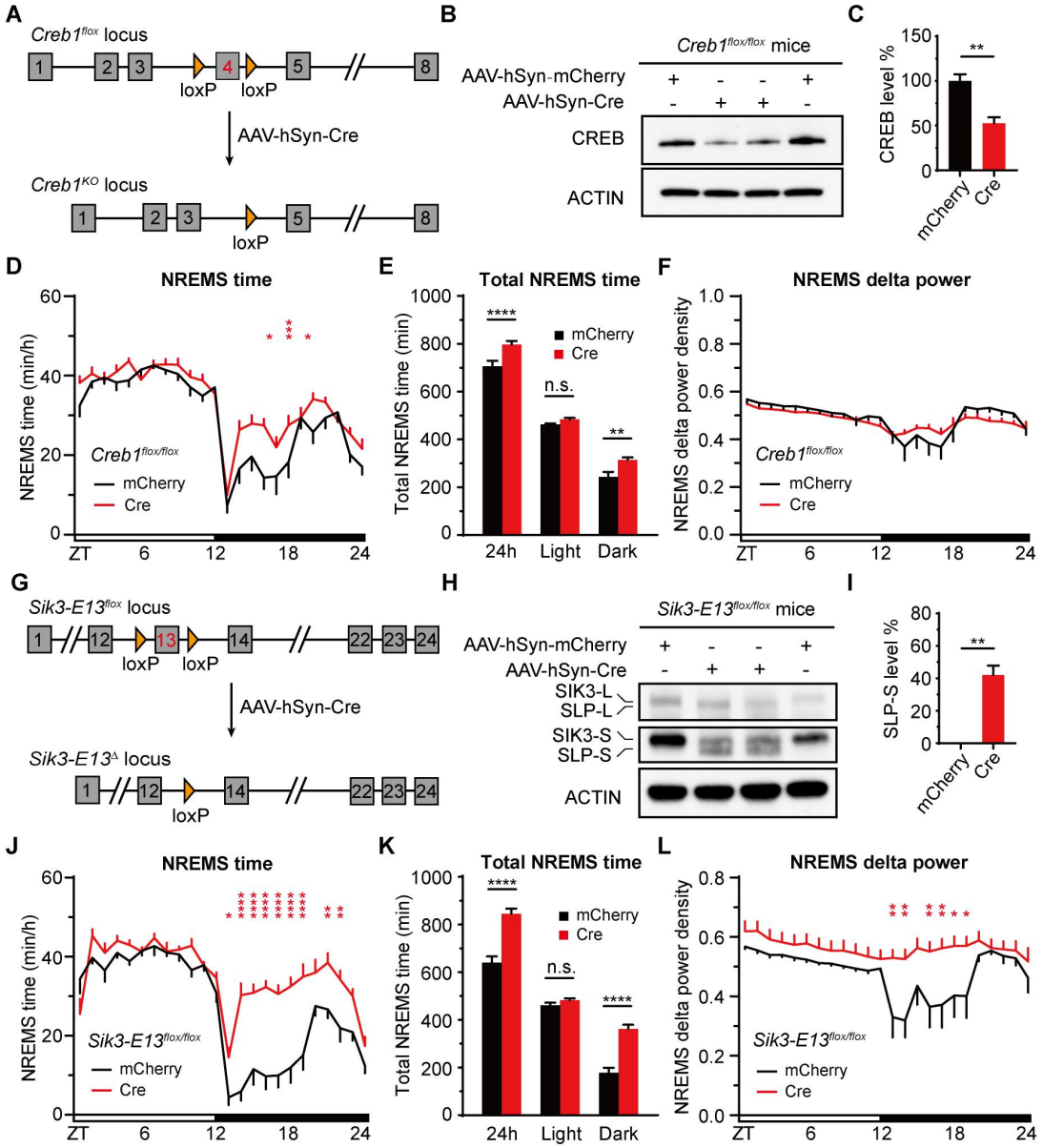

904 **Figure 4. ABC-KO of *Creb1* or exon 13 of *Sik3* by Cre-loxP recombination causes**
905 **hypersomnia.**
906 **(A)** Schematic of ABC-KO of *Creb1* by AAV-hSyn-Cre injection of *Creb1*$^{flox/flox}$ mice.
907 **(B)** Immunoblotting of whole brain lysates from AAV-hSyn-mCherry or AAV-hSyn-Cre injected
908 *Creb1*$^{flox/flox}$ mice with anti-CREB and anti-ACTIN antibodies.
909 **(C)** Quantification of the level of CREB expression in (B) (n=4).
910 **(D-F)** Hourly plot of NREMS time (D), quantification of total NREMS time (E) and hourly plot of
911 NREMS delta power (F) in the AAV-hSyn-mCherry (n=9) or AAV-hSyn-Cre (n=14) injected
912 *Creb1*$^{flox/flox}$ mice.
913 **(G)** Schematic of ABC-KO of exon 13 of *Sik3* by AAV-hSyn-Cre injection of *Sik3-E13*$^{flox/flox}$ mice.
914 **(H)** Immunoblotting of whole brain lysates from AAV-hSyn-mCherry or AAV-hSyn-Cre injected
915 *Sik3-E13*$^{flox/flox}$ mice with anti-SIK3 and anti-ACTIN antibodies.
916 **(I)** Quantification of the level of SLP-S expression in (H) (n=4), which is calculated by the
917 percentage of SLP-S/(SIK3-S+SLP-S).
918 **(J-L)** Hourly plot of NREMS time (J), quantification of total NREMS time (K) and hourly plot of
919 NREMS delta power (L) in the AAV-hSyn-mCherry (n=8) or AAV-hSyn-Cre (n=8) injected
920 *Sik3-E13*$^{flox/flox}$ mice.
921 Data are mean ± s.e.m. (C and I) Unpaired t test. (D-F) and (J-L) Two-way ANOVA with Tukey's
922 test. n.s. not significant; * $p < 0.05$; ** $p < 0.01$; *** $p < 0.001$; **** $p < 0.0001$.
923

Figure 5. Both long and short isoforms of Slp kinase contribute to hypersomnia of *Sik3*$^{Slp/+}$ mice.

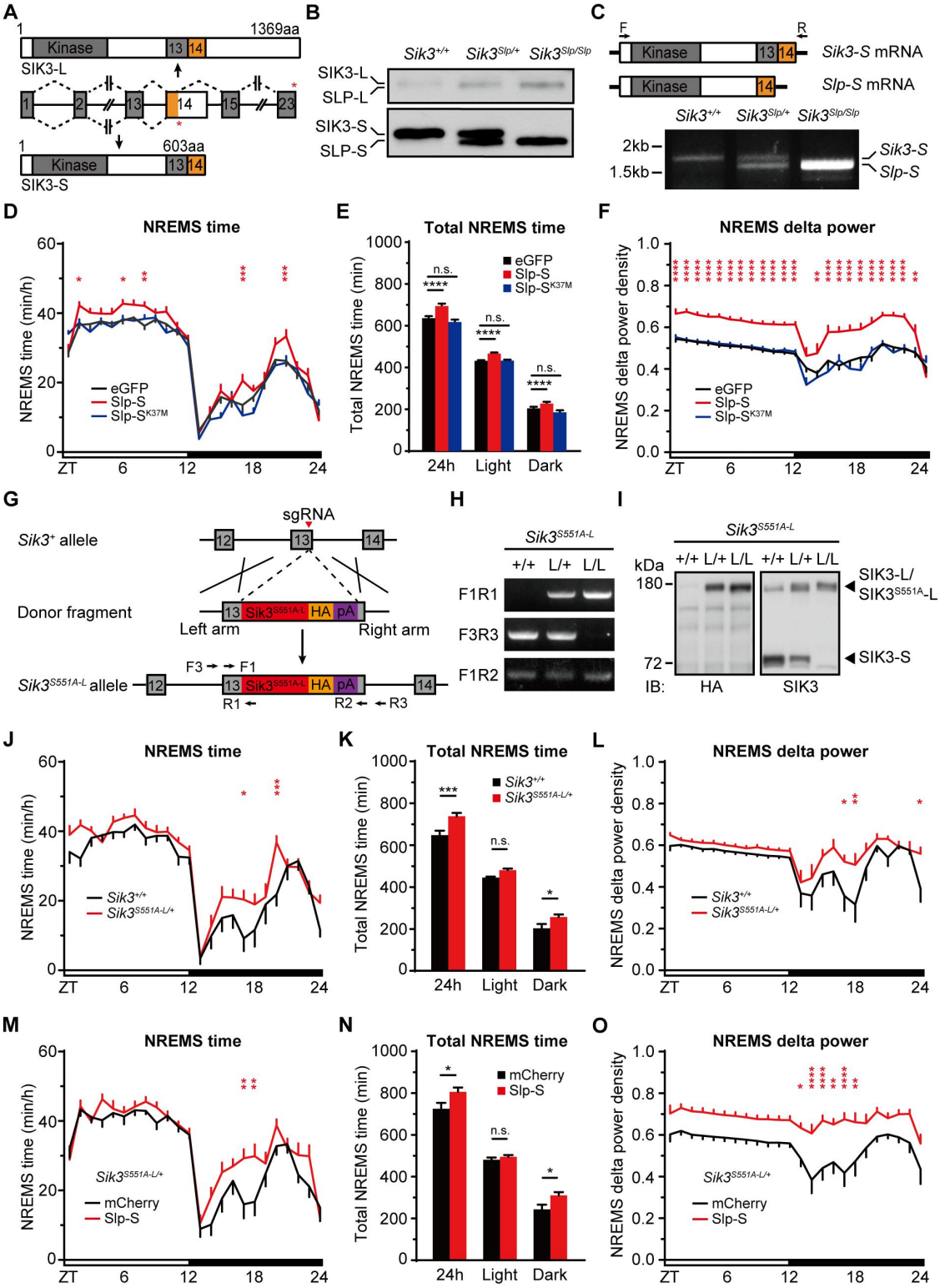

924

925

926

927

928 **Figure 5. Both short and long isoforms of SLP kinase contribute to hypersomnia of *Sik3^{Slp}***
929 **mice.**

930 **(A)** Schematic of alternative splicing of exon 14 to produce SIK3-L and SIK3-S protein isoforms.
931 Exons are shown as boxes and introns as lines. Red star refers to stop codon.

932 **(B)** Immunoblotting of whole brain lysates of *Sik3$^{+/+}$*, *Sik3$^{Slp/+}$* and *Sik3$^{Slp/Slp}$* mice with anti-SIK3
933 antibodies.

934 **(C)** RT-PCR analysis of the endogenous *Sik3-S* and *Slp-S* transcripts from the *Sik3$^{+/+}$*, *Sik3$^{Slp/+}$* and
935 *Sik3$^{Slp/Slp}$* mouse brains. Schematic of *Sik3-S* and *Slp-S mRNA* and PCR primers are shown
936 above.

937 **(D-F)** Hourly plot of NREMS time (D), quantification of total NREMS time (E) and hourly plot of
938 NREMS delta power (F) in the ABC-eGFP (black, n=27), ABC-Slp-S (red, n=23) and ABC-
939 Slp-S^{K37M} (blue, n=24) mice. (D and F) Shown above is the statistical analysis for comparison
940 between ABC-Slp-S mice and ABC-eGFP mice.

941 **(G)** Schematic for construction of *Sik3$^{S551A-L}$* mice by CRISPR/Cas9 and homologous
942 recombination.

943 **(H)** PCR genotyping of wild-type, heterozygous and homozygous *Sik3$^{S551A-L}$* knockin mice.

944 **(I)** Immunoblotting of brain extracts from wild-type, heterozygous and homozygous *Sik3$^{S551A-L}$*
945 mice with anti-HA and anti-SIK3 antibodies.

946 **(J-L)** Hourly plot of NREMS time (J), quantification of total NREMS time (K) and hourly plot of
947 NREMS delta power (L) of wild-type (*Sik3$^{+/+}$*, n=8) and heterozygous (*Sik3$^{S551A-L/+}$*, n=12)
948 littermates.

949 **(M-O)** Hourly plot of NREMS time (M), quantification of total NREMS time (N) and hourly plot
950 of NREMS delta power (O) in the AAV-hSyn-mCherry (n=12) or AAV-hSyn-Slp-S (Slp-S)
951 (n=12) injected *Sik3$^{S551A-L/+}$* mice.

Data are mean ± s.e.m. (D-F) and (J-O) Two-way ANOVA with Tukey's test; n.s. not significant; * $p < 0.05$; ** $p < 0.01$; *** $p < 0.001$; **** $p < 0.0001$.

Figure 6. ABC-KO of *NeuN* by triple-target CRISPR in Cas9 mice.

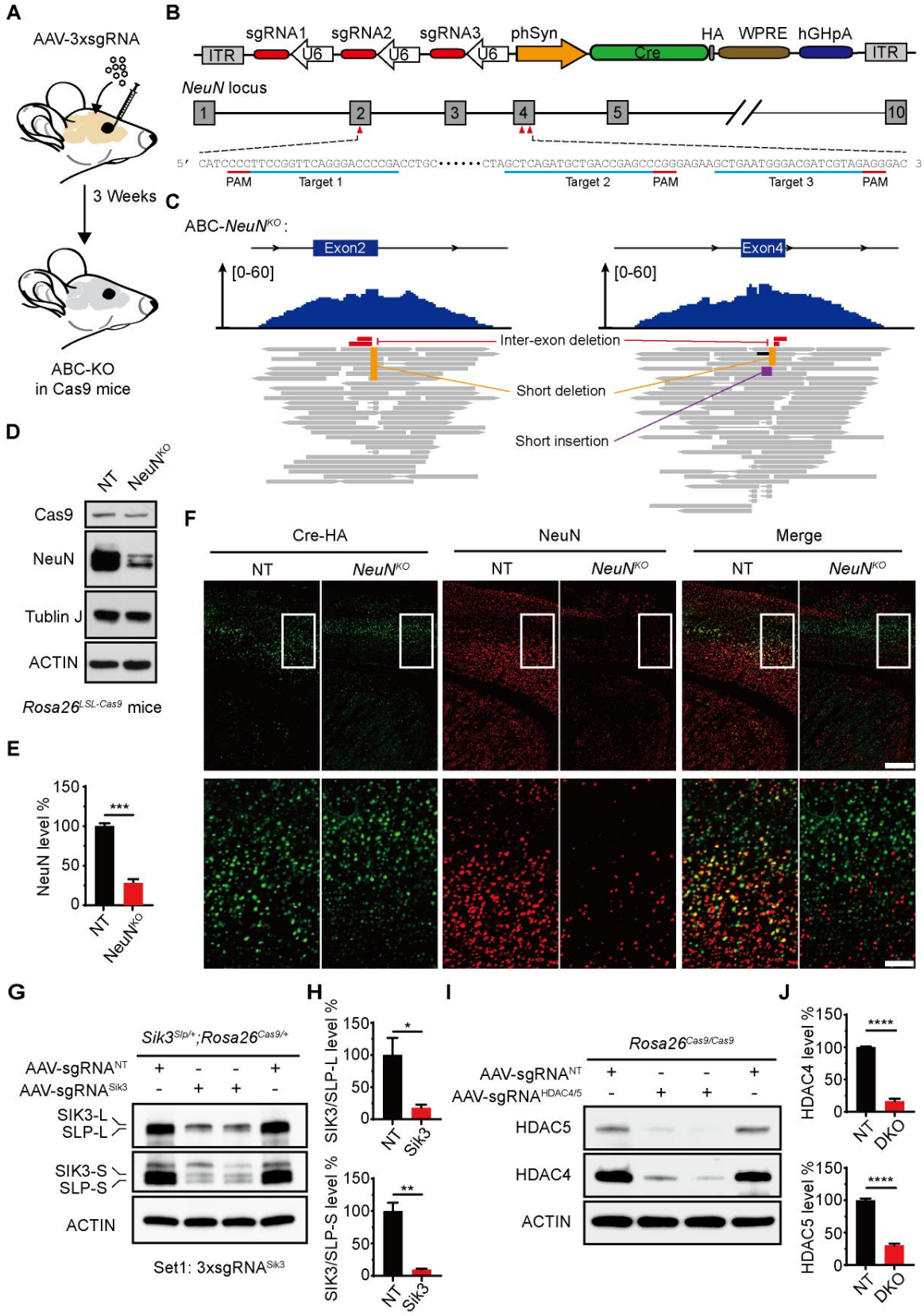

958 **Figure 6. ABC-KO of specific genes by triple-target CRISPR in Cas9 mice.**

959 **(A)** Schematic of ABC-KO of genes by triple-target CRISPR in *Rosa26*$^{LSL\text{-}Cas9}$ mice by retro-orbital
960 injection of AAV-PHP.eB expressing three sgRNAs targeting the same gene.

961 **(B)** Schematic of AAV-3xsgRNA^{NeuN} that expresses HA-Cre recombinase from the hSyn promoter
962 and three sgRNA cistrons from the U6 promoter. Shown below is the target site sequences
963 within the exons 2 and 4 of *NeuN* gene.

964 **(C)** Genomic alignments of whole genome sequencing reads of ABC-*NeuN*^{KO} mouse brain DNA at
965 the target sites within the exons 2 and 4 of *NeuN* gene. The top and bottom panels show read
966 coverage and read alignments, respectively, with different types of mutations highlighted.

967 **(D)** Immunoblotting of whole brain lysates from AAV-3xsgRNA^{NT} and AAV-3xsgRNA^{NeuN}
968 injected *Rosa26*$^{LSL\text{-}Cas9}$ mice with the corresponding antibodies.

969 **(E)** Quantification of the level of NeuN expression in (D) (n=4).

970 **(F)** Co-immunostaining of HA-Cre and NeuN in the prefrontal cortex sections of AAV-
971 3xsgRNA^{NT} and AAV-3xsgRNA^{NeuN} injected mice. The bottom row shows magnified images
972 of the corresponding boxed regions in the top row. Scale bars, 400 μm (top) and 100 μm
973 (bottom).

974 **(G)** Immunoblotting of whole brain lysates from AAV-sgRNA^{NT} and AAV-sgRNA^{Sik3} (set 1 of
975 three sgRNAs) injected *Sik3*$^{Slp/+}$; *Rosa26*$^{Cas9/+}$ mice with anti-SIK3 and anti-ACTIN antibodies.

976 **(H)** Quantification of the levels of SIK3-L/SLP-L and SIK3-S/SLP-S proteins shown in (G) (n=4).

977 **(I)** Immunoblotting of whole brain lysates from AAV-sgRNA^{HDAC4} and AAV-sgRNA^{HDAC5}
978 injected *Rosa26*$^{Cas9/Cas9}$ mice with anti-HDAC4, Anti-HDAC5 and anti-ACTIN antibodies.

979 **(J)** Quantification of the levels of HDAC4 and HDAC5 proteins in (I) (n=4).

980 Data are mean ± s.e.m. (E, H and J) Unpaired t test. * $p < 0.05$; ** $p < 0.01$; *** $p < 0.001$; **** p
981 < 0.0001.

982

Figure 7. Multiplex ABC-KO of target genes cause various sleep phenotypes.

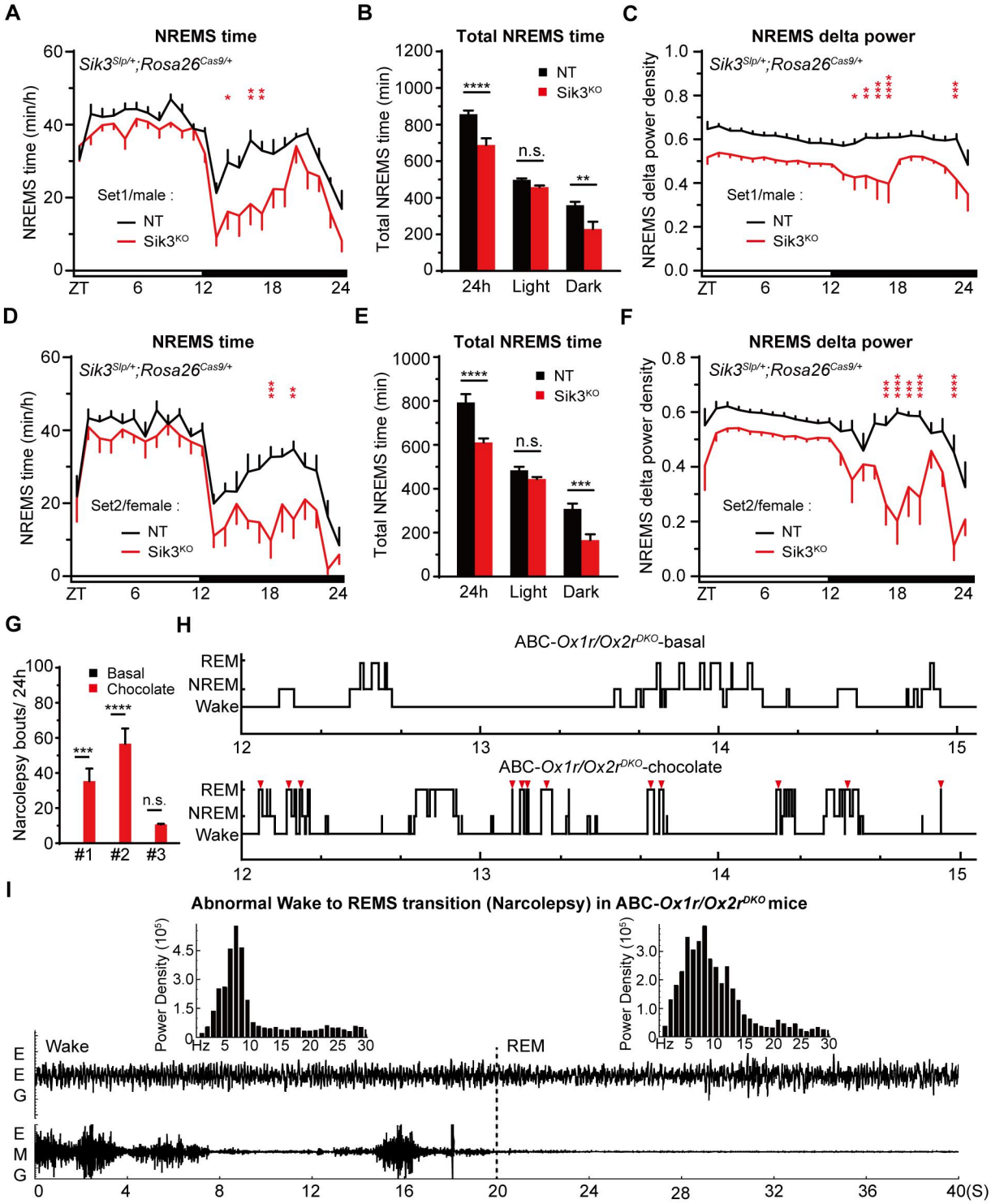

988 **Figure 7. Multiplex ABC-KO of genes by CRISPR/Cas9 causes various sleep phenotypes.**

989 **(A-C)** Hourly plot of NREMS time (A), quantification of total NREMS time (B) and hourly plot of
990 NREMS delta power (C) in the AAV-sgRNA^{NT} (n=7) or AAV-sgRNA^{Sik3} (set 1, n=7) injected
991 *Sik3*$^{Slp/+}$; *Rosa26*$^{Cas9/+}$ male mice.

992 **(D-F)** Hourly plot of NREMS time (D), quantification of total NREMS time (E) and hourly plot of
993 NREMS delta power (F) in the AAV-sgRNA^{NT} (n=7) or AAV-gRNA^{Sik3} (set 2, n=7) injected
994 *Sik3*$^{Slp/+}$; *Rosa26*$^{Cas9/+}$ female mice.

995 **(G)** Quantification of the number of narcolepsy episodes in three ABC-*Ox1r/Ox2r*^{DKO} mice before
996 and after chocolate feeding for three days.

997 **(H)** Representative hypnograms (ZT12-15) showing ABC-*Ox1r/Ox2r*^{DKO} mice before and after
998 chocolate feeding. Red triangles mark direct wake to REM transitions that are characteristic of
999 narcolepsy episodes.

1000 **(I)** Representative EEG/EMG signals depicting the abnormal wake to REM transition during one
1001 narcoleptic episode in ABC-*Ox1r/Ox2r*^{DKO} mice.

1002 Data are mean ± s.e.m. (A, C, D, F) Two-way ANOVA with Tukey's test. (B, E, G) Unpaired t test.
1003 n.s. not significant; * $p < 0.05$; ** $p < 0.01$; *** $p < 0.001$; **** $p < 0.0001$.

1004

1005

1006

1007

1008

1009

1010

1011

1012

1013

1014 **SUPPLEMENTARY FIGURE LEGEND**

Figure S1. Setup a video based high-throughput ABC sleep screening platform.

Linked to Figure 1

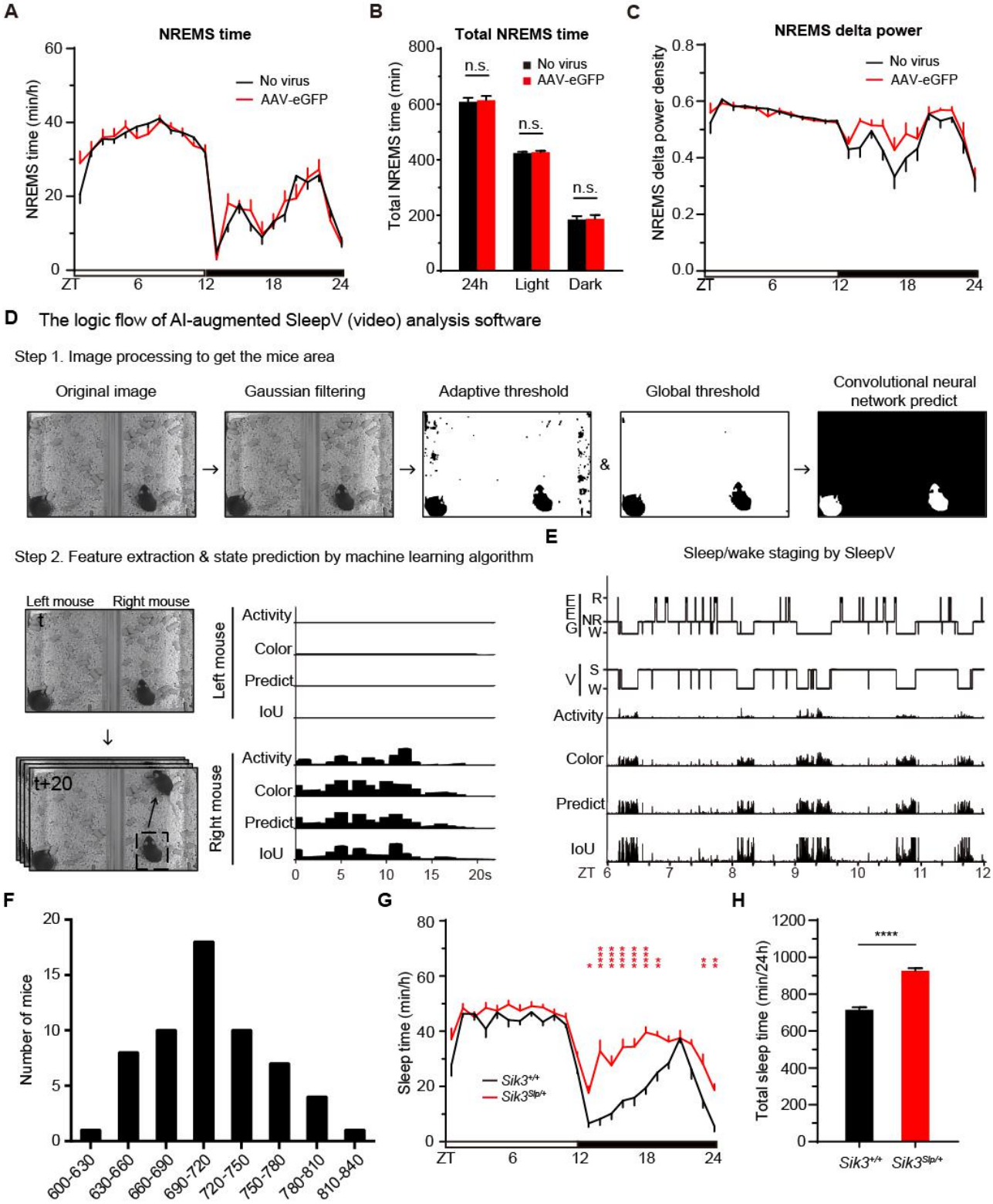

1015

1016

1017 **Figure S1. Setup of a video based high-throughput ABC-expression sleep screening platform.**

1018 **(Linked to Figure 1)**

1019 **(A-C)** Hourly plot of NREMS time (A), quantification of total NREMS time (B) and hourly plot of

1020 NREMS delta power (C) of no virus (n=19) or AAV-hSyn-eGFP (n=9) injected mice.

1021 **(D)** The logic flow of sleep/wake staging of video recording by SleepV software.

1022 **(E)** Epoch-by-epoch comparison of sleep/wake staging of the same mouse by simultaneous SleepV

1023 (V) and EEG/EMG recording and analysis.

1024 **(F)** The distribution of daily sleep time in fifty-nine C57BL/6J mice as measured by SleepV

1025 analysis.

1026 **(G)** Hourly plot of sleep time of *Sik3*$^{+/+}$ (n=11) and *Sik3*$^{Slp/+}$ (n=11) mice.

1027 **(H)** Quantification of daily sleep time in *Sik3*$^{+/+}$ (n=11) and *Sik3*$^{Slp/+}$ (n=11) mice.

1028 Data are mean ± s.e.m. (G) Two-way ANOVA with Tukey's test. (H) Unpaired t test. * $p < 0.05$;

1029 ** $p < 0.01$; **** $p < 0.0001$.

1030

1031

Figure S2. ABC-expression of CREB and/or CRTC1 reduces NREMS amount and delta power. Linked to Figure 2

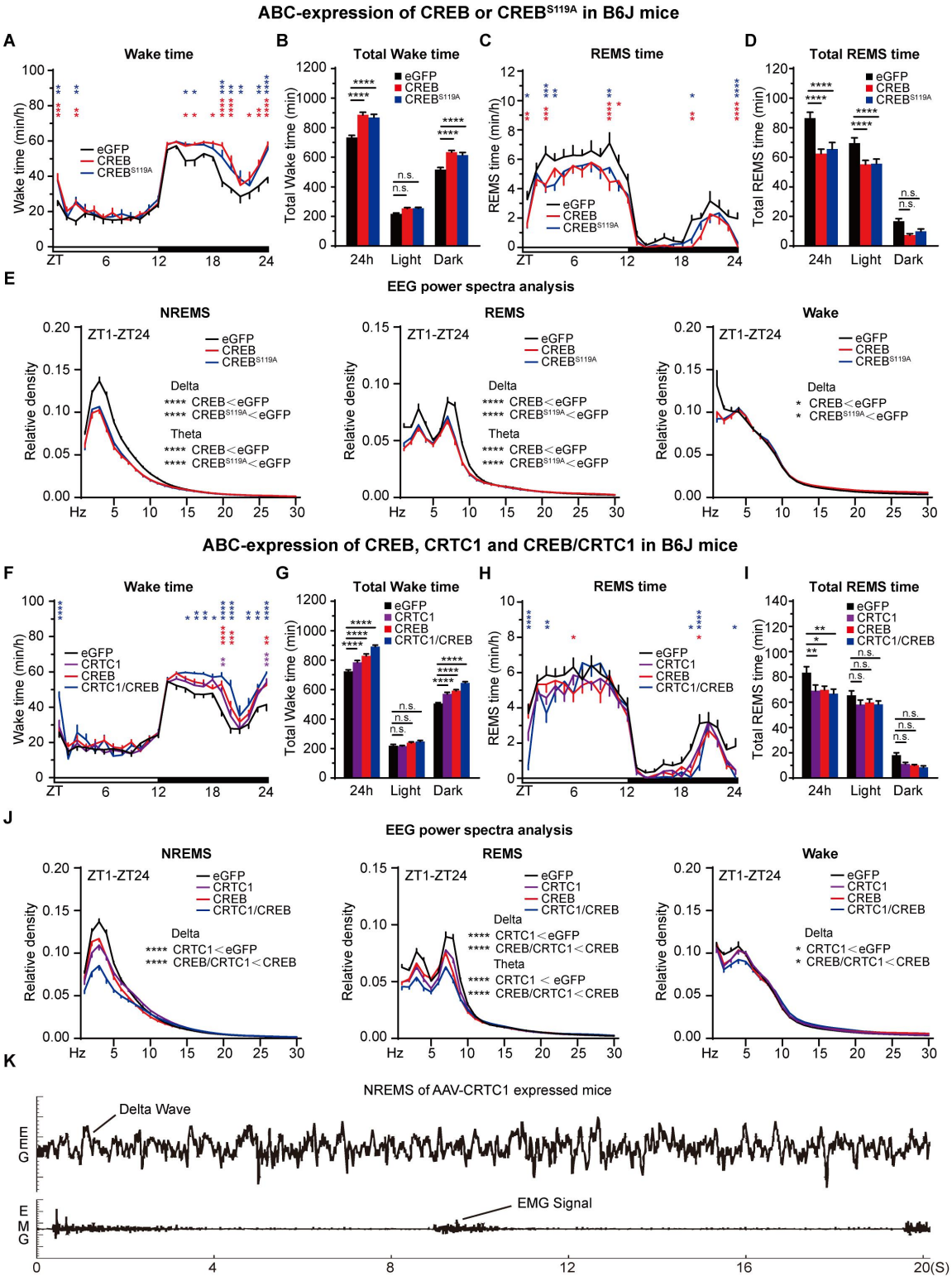

1035 **Figure S2. ABC-expression of CREB and/or CRTC1 reduces NREMS amount and delta**
1036 **power.**
1037 **(Linked to Figure 2)**
1038 **(A and B)** Hourly plot of wake time (A) and quantification of total wake time (B) in the ABC-
1039 eGFP (n=11), ABC-CREB$_{\Delta}$ (n=12) and ABC-CREB$_{\Delta}^{S119A}$ (n=11) mice. Shown above is
1040 statistical analysis for comparison between ABC-CREB (red*) or ABC-CREB^{S119A} (blue*) mice
1041 and control ABC-eGFP mice.
1042 **(C and D)** Hourly plot of REMS time (C) and quantification of total REMS time (D) in the ABC-
1043 eGFP, ABC-CREB$_{\Delta}$ and ABC-CREB$_{\Delta}^{S119A}$ mice.
1044 **(E)** EEG power spectra analysis of NREMS, REMS and wake in the ABC-eGFP, ABC-CREB$_{\Delta}$,
1045 and ABC-CREB$_{\Delta}^{S119A}$ mice.
1046 **(F and G)** Hourly plot of wake time (F) and quantification of total wake time (G) in ABC-eGFP
1047 (n=12), ABC-CRTC1 (n=15), ABC-CREB$_{\Delta}$ (n=15) and ABC-CRTC1/CREB$_{\Delta}$ (n=12) mice.
1048 Shown above is the statistical analysis for comparison between ABC-CRTC1 (purple*), ABC-
1049 CREB$_{\Delta}$ (red*), or ABC-CRTC1/CREB$_{\Delta}$ (blue*) mice and control ABC-eGFP mice.
1050 **(H and I)** Hourly plot of REMS time (H) and quantification of total REMS time (I) in the ABC-
1051 eGFP, ABC-CRTC1, ABC-CREB$_{\Delta}$ and ABC-CRTC1/CREB$_{\Delta}$ mice.
1052 **(J)** EEG power spectra analysis of NREMS, REMS and wake in the ABC-eGFP, ABC-CRTC1,
1053 ABC-CREB$_{\Delta}$ and ABC-CRTC1/CREB$_{\Delta}$ mice.
1054 **(K)** Representative EEG/EMG hypnogram depicting frequent muscle twitching during NREMS in
1055 the ABC-CRTC1 mice.
1056 Data are mean ± s.e.m. (A-J) Two-way ANOVA with Tukey's test. n.s. not significant; * $p < 0.05$;
1057 ** $p < 0.01$; *** $p < 0.001$; **** $p < 0.0001$.
1058
1059
1060

Figure S3. Inducible ABC-expression of CREB^{VP16} or CRTC1^{CA} causes significant sleep phenotypes. Linked to Figure 3

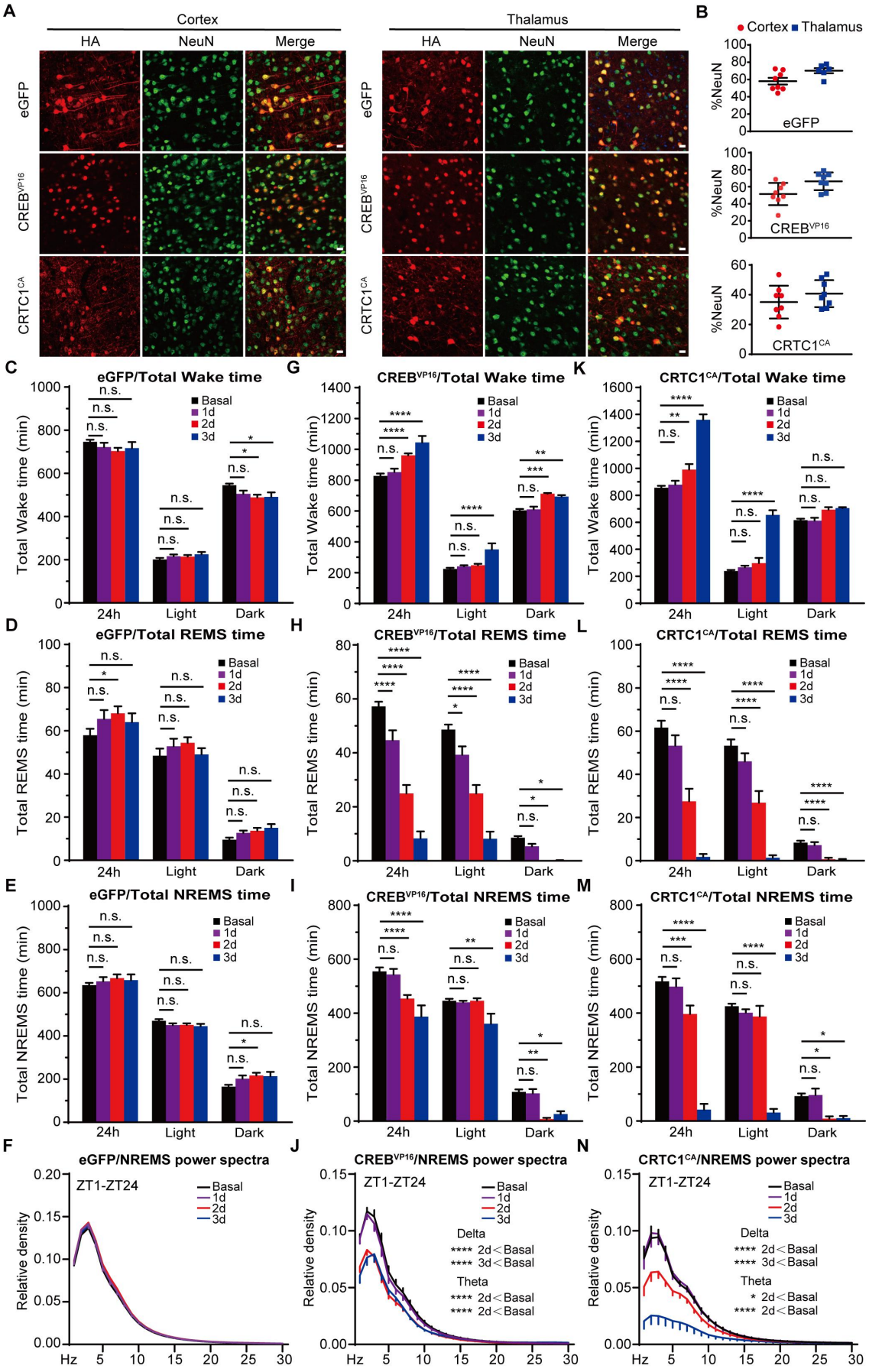

1061

1062 **Figure S3. Inducible ABC-expression of CREB^{VP16} or CRTC1^{CA} causes significant sleep**
1063 **phenotypes. (Linked to Figure 3)**

1064 **(A)** Co-immunostaining of HA^{+} (red) and NeuN^{+} (green) neurons in the cortex and thalamus of the
1065 the inducible (i) ABC-eGFP, ABC-CREB^{VP16} and ABC-CRTC1^{CA} mice.

1066 **(B)** Quantification of the viral transduction rates, which is calculated by the percentage of NeuN^{+}
1067 neurons that express HA-tagged proteins, in the cortical and thalamic neurons showed in (A).

1068 **(C-F)** Quantification of total wake time (C), REMS time (D), or NREMS time (E) and EEG power
1069 spectra analysis of NREMS (F) in the iABC-eGFP mice (n=8).

1070 **(G-J)** Quantification of total wake time (G), REMS time (H), or NREMS time (I) and EEG power
1071 spectra analysis of NREMS (J) in the iABC-CREB^{VP16} mice (n=7).

1072 **(K-N)** Quantification of total wake time (K), REMS time (L), or NREMS time (M) and EEG power
1073 spectra analysis of NREMS (N) in the iABC-CRTC1^{CA} mice (n=7).

1074 Data are mean ± s.e.m. (C-N) Two-way ANOVA with Tukey's test. n.s. not significant; * p <0.05;
1075 ** $p < 0.01$; *** $p < 0.001$; **** $p < 0.0001$.

1076

Figure S4. ABC-KO of *Creb1* or exon 13 of *Sik3* by Cre-loxP recombination causes hypersomnia. Linked to Figure 4

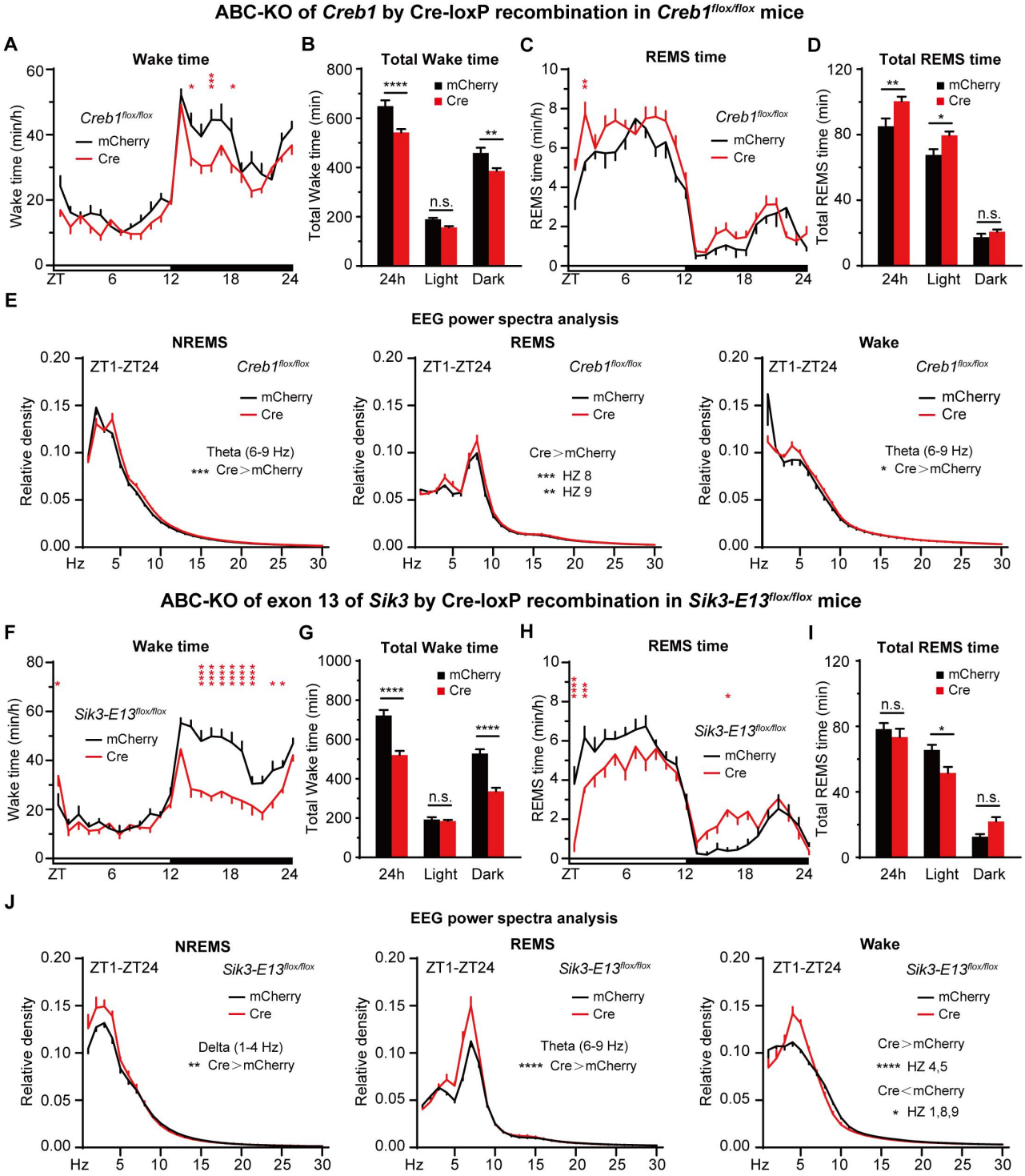

1082 **Figure S4. ABC-KO of *Creb1* or exon 13 of *Sik3* by Cre-loxP recombination causes**
1083 **hypersomnia. (Linked to Figure 4)**

1084 **(A and B)** Hourly plot of wake time (A) and quantification of total wake time (B) in the AAV-
1085 hSyn-mCherry (n=9) or AAV-hSyn-Cre (n=14) injected *Creb1*$^{flox/flox}$ mice.

1086 **(C and D)** Hourly plot of REMS time (C) and quantification of total REMS time (D) in the AAV-
1087 hSyn-mCherry or AAV-hSyn-Cre injected *Creb1*$^{flox/flox}$ mice.

1088 **(E)** EEG power spectra analysis of NREMS, REMS and wake in the AAV-hSyn-mCherry or AAV-
1089 hSyn-Cre injected *Creb1*$^{flox/flox}$ mice.

1090 **(F and G)** Hourly plot of wake time (F) and quantification of total wake time (G) in the AAV-
1091 hSyn-mCherry (n=8) or AAV-hSyn-Cre (n=8) injected *Sik3-E13*$^{flox/flox}$ mice.

1092 **(H and I)** Hourly plot of REMS time (H) and quantification of total REMS time (I) in the AAV-
1093 hSyn-mCherry or AAV-hSyn-Cre injected *Sik3-E13*$^{flox/flox}$ mice.

1094 **(J)** EEG power spectra analysis of NREMS, REMS and wake in the AAV-hSyn-mCherry or AAV-
1095 hSyn-Cre injected *Sik3-E13*$^{flox/flox}$ mice.

1096 Data are mean ± s.e.m. (A-J) Two-way ANOVA with Tukey's test. n.s. not significant; * p <0.05;
1097 ** $p < 0.01$; *** $p < 0.001$; **** $p < 0.0001$.

1098

1099

Figure S5. ABC-expression of Slp-S causes mild hypersomnia in a kinase-dependent manner. Linked to Figure 5

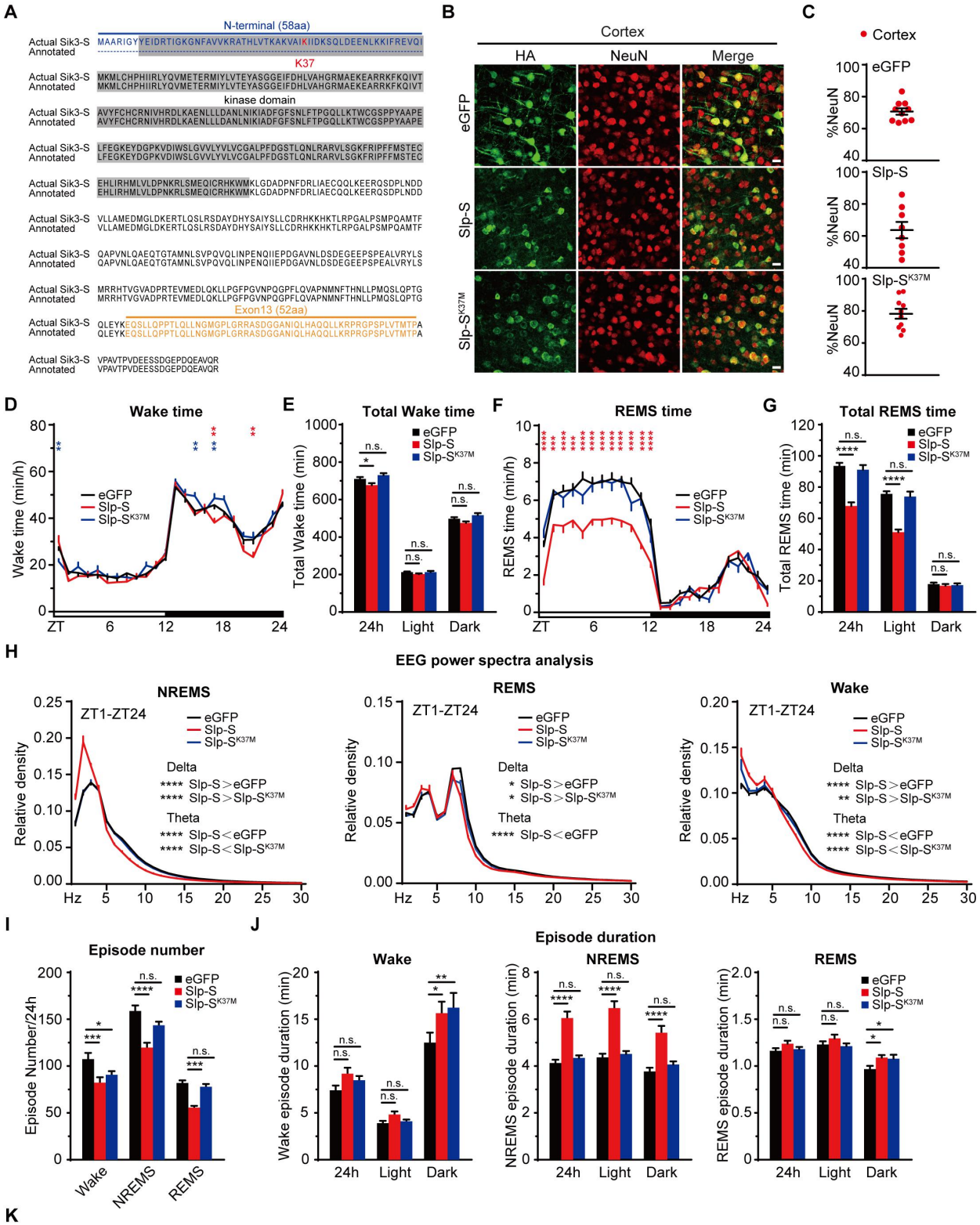

1100

1101 **Figure S5. ABC-expression of Slp-S causes mild hypersomnia in a kinase-dependent manner.**
1102 **(Linked to Figure 5)**

1103 **(A)** Alignment of the actual and annotated (Uniprot F6U8X4) SIK3-S protein sequences.
1104 Highlighted are the N-terminal 58 amino acids (blue), protein kinase domain (gray), K37 (red)
1105 and 52 amino acids (orange) encoded by exon 13 of *Sik3*.

1106 **(B)** Representative images showing co-immunostaining of HA (green) and NeuN (red) of the cortex
1107 of the ABC-eGFP, ABC-Slp-S and ABC-Slp-S^{K37M} mouse brains. Scale bars, 20um.

1108 **(C)** Quantification of the viral transduction rates of the cortical neurons in (B), which is calculated
1109 by the percentage of $NeuN^{+}$ neurons that express HA-tagged proteins, in the ABC-eGFP, ABC-
1110 Slp-S and ABC-Slp-S^{K37M} mouse brains.

1111 **(D and E)** Hourly plot of wake time (D) and quantification of total wake time (E) in the ABC-
1112 eGFP (black, n=27), ABC-Slp-S (blue, n=23) and ABC-Slp-S^{K37M} (purple, n=24) mice.

1113 **(F and G)** Hourly plots of REMS time (F) and quantification of total REMS time (G) in the ABC-
1114 eGFP, ABC-Slp-S and ABC-Slp-S^{K37M} mice.

1115 **(H)** EEG power spectra analysis of NREMS, REMS and wake in the ABC-eGFP, ABC-Slp-S and
1116 ABC-Slp-S^{K37M} mice.

1117 **(I)** Quantitation of daily NREMS, REMS or wake episode number in the ABC-eGFP, ABC-Slp-S,
1118 and ABC-Slp-S^{K37M} mice.

1119 **(J)** Comparison of mean episode duration of wake, NREMS, or REMS in ABC-eGFP, ABC-Slp-S,
1120 and ABC-Slp-S^{K37M} mice during the 24-h cycle.

1121 **(K)** Comparison of the frequency of transitions among the wake, NREMS and REMS states
1122 between the ABC-Slp-S or ABC-Slp-S^{K37M} mice and control ABC-eGFP mice.

1123 Data are mean±s.e.m. (D-K) Two-way ANOVA with Tukey's test. n.s. not significant; * $p<0.05$;
1124 ** $p<0.01$; *** $p<0.001$; **** $p<0.0001$.

1125

1126

Figure S6. Both long and short isoforms of Slp kinase contribute to hypersomnia of *Sik3*$^{Slp/+}$ mice. Linked to Figure 5

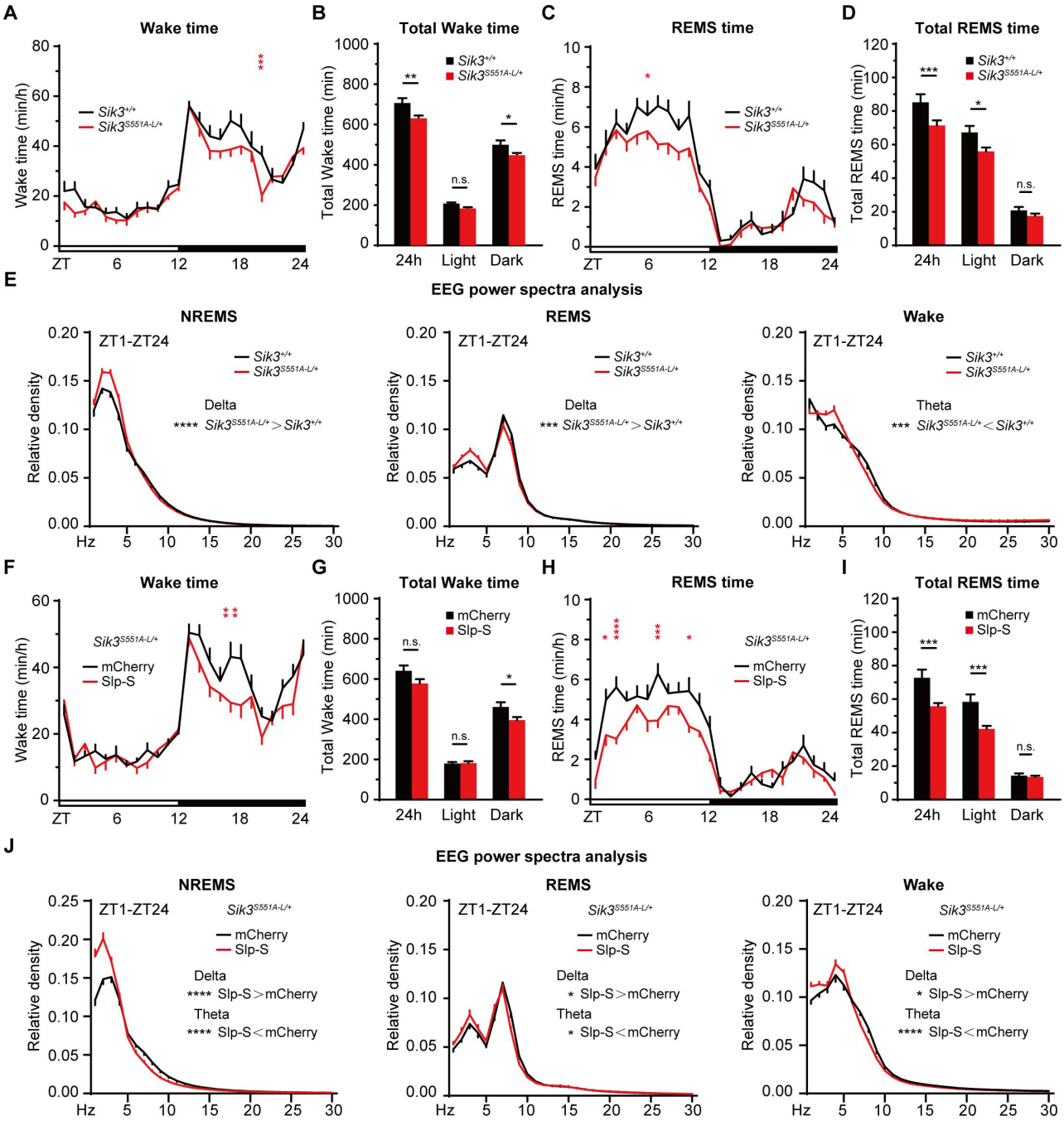

1133 **Figure S6. Both long and short isoforms of SLP contribute to hypersomnia of *Sik3*$^{Slp/+}$ mice.**

1134 **(Linked to Figure 5)**

1135 **(A and B)** Hourly plot of wake time (A) and quantification of total wake time (B) in the wild-type

1136 (*Sik3*$^{+/+}$, n=8) and heterozygous (*Sik3*$^{S551A\text{-}L/+}$, n=12) mice.

1137 **(C and D)** Hourly plot of REMS time (C) and quantification of total REMS time (D) in the wild-

1138 type and heterozygous *Sik3*$^{S551A\text{-}L}$ mice.

1139 **(E)** EEG power spectra analysis of wake, NREMS and REMS states (ZT1-24) in the wild-type

1140 and heterozygous *Sik3*$^{S551A\text{-}L}$ mice.

1141 **(F and G)** Hourly plot of wake time (F) and quantification of total wake time (G) in the AAV-

1142 hSyn-mCherry (n=8) or AAV-hSyn-Slp-S (n=8) injected heterozygous *Sik3*$^{S551A\text{-}L}$ (*Sik3*$^{S551A\text{-}L/+}$)

1143 mice.

1144 **(H and I)** Hourly plot of REMS time (H) and quantification of total REMS time (I) in the AAV-

1145 hSyn-mCherry or AAV-hSyn-Slp-S injected heterozygous *Sik3*$^{S551A\text{-}L}$ mice.

1146 **(J)** EEG power spectra analysis of wake, NREMS and REMS states in the AAV-hSyn-mCherry or

1147 AAV-hSyn-Slp-S injected heterozygous *Sik3*$^{S551A\text{-}L}$ mice.

1148 Data are mean ± s.e.m. (A-J) Two-way ANOVA with Tukey's test. n.s. not significant; * $p < 0.05$;

1149 ** $p < 0.01$; *** $p < 0.001$; **** $p < 0.0001$.

1150

1151

1152

Figure S7. ABC-KO of target genes by triple-target CRISPR in *Cas9* mice.
Linked to Figure 6

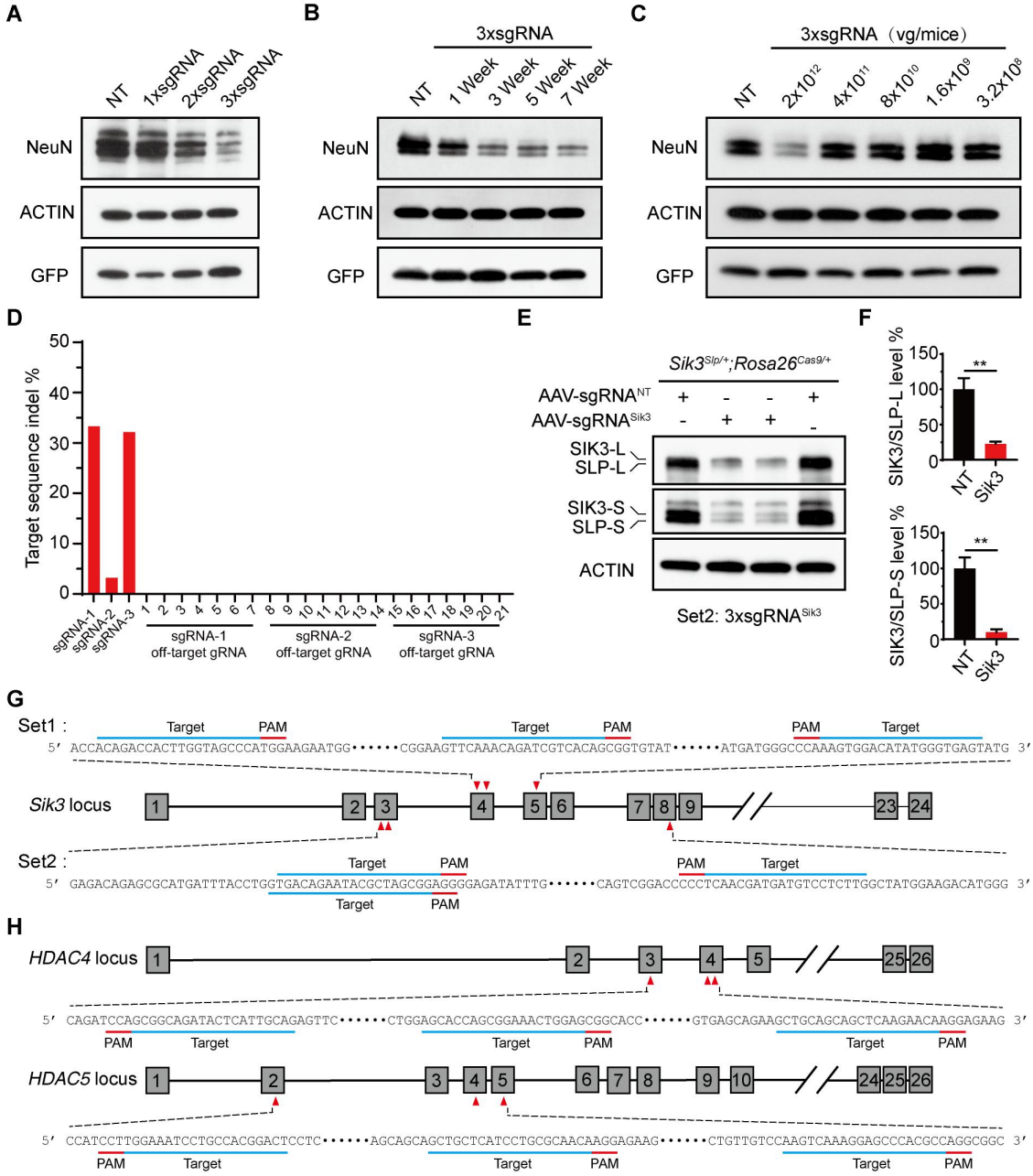

1153

1154

1155

1156

1157

1158

1159

1160 **Figure S7. ABC-KO of specific genes by triple-target CRISPR in *Cas9* mice.**

1161 **(Linked to Figure 6)**

1162 **(A)** Immunoblotting of NeuN proteins in whole brain lysates from AAV-3xsgRNA^{NT}, AAV-1xsg

1163 RNA^{NeuN}, AAV-2xsgRNA^{NeuN}, AAV-3xsgRNA^{NeuN} injected *Rosa26*$^{LSL\text{-}Cas9\text{-}IRES\text{-}EGFP}$ mice at

1164 three weeks after (10^{12} vg/mice) virus injection. β-ACTIN was used as loading control and GFP

1165 as indicator for Cas9 expression.

1166 **(B)** Immunoblotting of NeuN proteins in whole brain lysates from AAV-3xsgRNA^{NeuN} injected

1167 Cas9 mice at one, three, five and seven weeks after virus (10^{12} vg/mice) injection. AAV-

1168 3xsgRNA^{NT} injected mouse brains were collected at three weeks after virus injection.

1169 **(C)** Immunoblotting of NeuN proteins in whole brain lysates from Cas9 mice injected with

1170 increasing doses of AAV-3xsgRNA^{NeuN} and collected at three weeks after virus injection. The

1171 dose of AAV-3xsgRNA^{NT} injection was $2x10^{12}$ vg/mice.

1172 **(D)** Quantitation of indel mutations at the three target sites and twenty-one predicted off-target sites

1173 for the three sgRNAs targeting *NeuN* gene based on the whole genome sequencing data.

1174 **(E)** Immunoblotting of whole brain lysates from AAV-sgRNA^{NT} and AAV-sgRNA^{Sik3} (set 2 of

1175 three sgRNAs) injected *Sik3*$^{Slp/+}$; *Rosa26*$^{Cas9/+}$ mice with anti-SIK3 and anti-ACTIN antibodies.

1176 **(F)** Quantification of the levels of SIK3-L/SLP-L and SIK3-S/SLP-S proteins shown in (E) (n=4).

1177 **(G)** Schematic of the two sets of three sgRNAs targeting different exons of the *Sik3* gene.

1178 **(H)** Schematic of separate sets three sgRNAs targeting the *Hdac4* or *Hdac5* gene, respectively.

1179 Data are mean ± s.e.m. (F) Unpaired t test. ** $p < 0.01$.

1180

1181

Figure S8. ABC-KO of *Slp/Sik3* alleles rescues hypersomnia of *Sik3*$^{Slp/+}$;*Rosa26*$^{Cas9/+}$ mice. Linked to Figure 7

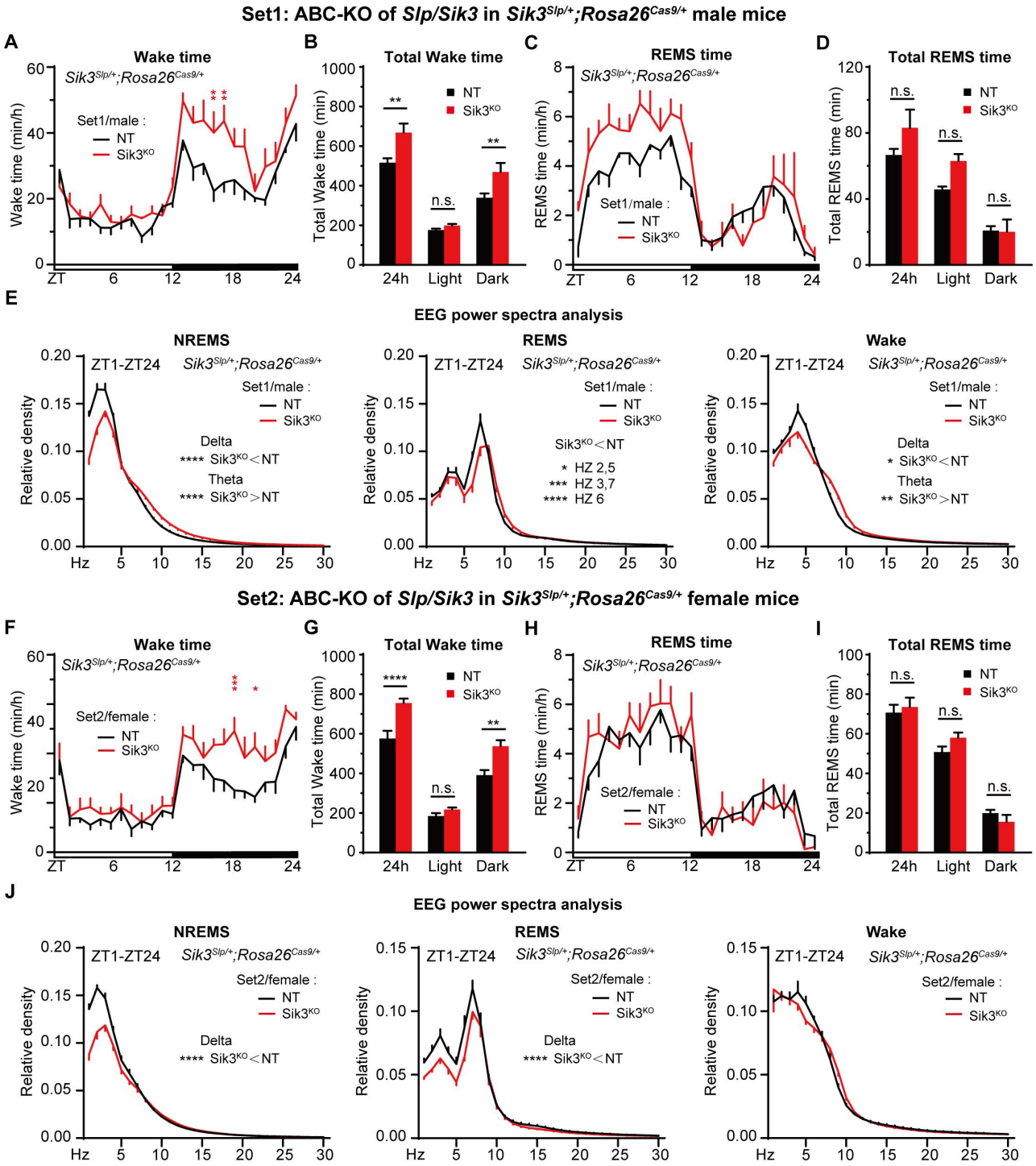

1182

1183

1184

1185

1186

1187 **Figure S8. Multiplex ABC-KO by CRISPR/Cas9 causes various sleep phenotypes.**

1188 **(Linked to Figure 7)**

1189 **(A and B)** Hourly plot of wake time (A) and quantification of total wake time (B) in the AAV-

1190 sgRNA^{NT} (n=7) or AAV-sgRNA^{Sik3} (set 1, n=7) injected *Sik3*$^{Slp/+}$; *Rosa26*$^{Cas9/+}$ male mice.

1191 **(C and D)** Hourly plot of REMS time (C) and quantification of total REMS time (D) in the AAV-

1192 sgRNA^{NT} or AAV-sgRNA^{Sik3} (set 1, n=7) injected *Sik3*$^{Slp/+}$; *Rosa26*$^{Cas9/+}$ male mice.

1193 **(E)** EEG power spectra analysis of NREMS, REMS and wake states in the AAV-sgRNA^{NT} or

1194 AAV-sgRNA^{Sik3} injected *Sik3*$^{Slp/+}$; *Rosa26*$^{Cas9/+}$ male mice.

1195 **(F and G)** Hourly plot of wake time (F) and quantification of total wake time (G) in the AAV-

1196 sgRNA^{NT} (n=6) or AAV-sgRNA^{Sik3} (set 2, n=7) injected *Sik3*$^{Slp/+}$; *Rosa26*$^{Cas9/+}$ female mice.

1197 **(H and I)** Hourly plot of REMS time (H) and quantification of total REMS time (I) in the AAV-

1198 sgRNA^{NT} (n=6) or AAV-sgRNA^{Sik3} (set 2, n=7) injected *Sik3*$^{Slp/+}$; *Rosa26*$^{Cas9/+}$ female mice.

1199 **(J)** EEG power spectra analysis of NREMS, REMS and wake states in the AAV-sgRNA^{NT} or

1200 AAV-sgRNA^{Sik3} injected *Sik3*$^{Slp/+}$; *Rosa26*$^{Cas9/+}$ female mice.

1201 Data are mean ± s.e.m. (A-J) Two-way ANOVA with Tukey's test. n.s. not significant; * $p < 0.05$;

1202 ** $p < 0.01$; *** $p < 0.001$; **** $p < 0.0001$.

1203

1204 **REFERENCES**

1205 Banks, G.T., Guillaumin, M.C.C., Heise, I., Lau, P., Yin, M., Bourbia, N., Aguilar, C., Bowl, M.R.,
1206 Esapa, C., Brown, L.A., *et al.* (2020). Forward genetics identifies a novel sleep mutant with sleep
1207 state inertia and REM sleep deficits. Science Advances *6*, eabb3567.

1208 Barco, A., Alarcon, J.M., and Kandel, E.R. (2002). Expression of constitutively active CREB
1209 protein facilitates the late phase of long-term potentiation by enhancing synaptic capture. Cell *108*,
1210 689-703.

1211 Benito, E., and Barco, A. (2010). CREB's control of intrinsic and synaptic plasticity: implications
1212 for CREB-dependent memory models. Trends in Neurosciences *33*, 230-240.

1213 Bentivoglio, M., and Grassi-Zucconi, G. (1997). The pioneering experimental studies on sleep
1214 deprivation. Sleep *20*, 570-576.

1215 Bibb, J.A. (2003). Role of Cdk5 in neuronal signaling, plasticity, and drug abuse. Neuro-Signals *12*,
1216 191-199.

1217 Bleckmann, S.C., Blendy, J.A., Rudolph, D., Monaghan, A.P., Schmid, W., and Schutz, G. (2002).
1218 Activating transcription factor 1 and CREB are important for cell survival during early mouse
1219 development. Molecular and Cellular Biology *22*, 1919-1925.

1220 Borel, F., Kay, M.A., and Mueller, C. (2014). Recombinant AAV as a platform for translating the
1221 therapeutic potential of RNA interference. Molecular Therapy *22*, 692-701.

1222 Carmany-Rampey, A., and Moens, C.B. (2006). Modern mosaic analysis in the zebrafish. Methods
1223 *39*, 228-238.

1224 Ch'ng, T.H., Uzgil, B., Lin, P., Avliyakulov, N.K., O'Dell, T.J., and Martin, K.C. (2012). Activity-
1225 dependent transport of the transcriptional coactivator CRTC1 from synapse to nucleus. Cell *150*,
1226 207-221.

1227 Chan, K.Y., Jang, M.J., Yoo, B.B., Greenbaum, A., Ravi, N., Wu, W.L., Sanchez-Guardado, L.,
1228 Lois, C., Mazmanian, S.K., Deverman, B.E., *et al.* (2017). Engineered AAVs for efficient

1229 noninvasive gene delivery to the central and peripheral nervous systems. Nature Neuroscience *20*,
1230 1172-1179.
1231 Chemelli, R.M., Willie, J.T., Sinton, C.M., Elmquist, J.K., Scammell, T., Lee, C., Richardson, J.A.,
1232 Williams, S.C., Xiong, Y., Kisanuki, Y.*, et al.* (1999). Narcolepsy in orexin knockout mice:
1233 molecular genetics of sleep regulation. Cell *98*, 437-451.
1234 Choudhury, S.R., Harris, A.F., Cabral, D.J., Keeler, A.M., Sapp, E., Ferreira, J.S., Gray-Edwards,
1235 H.L., Johnson, J.A., Johnson, A.K., Su, Q.*, et al.* (2016). Widespread Central Nervous System
1236 Gene Transfer and Silencing After Systemic Delivery of Novel AAV-AS Vector. Molecular
1237 Therapy *24*, 726-735.
1238 Chowdhury, S., Shepherd, J.D., Okuno, H., Lyford, G., Petralia, R.S., Plath, N., Kuhl, D., Huganir,
1239 R.L., and Worley, P.F. (2006). Arc/Arg3.1 interacts with the endocytic machinery to regulate
1240 AMPA receptor trafficking. Neuron *52*, 445-459.
1241 Chrivia, J.C., Kwok, R.P., Lamb, N., Hagiwara, M., Montminy, M.R., and Goodman, R.H. (1993).
1242 Phosphorylated CREB binds specifically to the nuclear protein CBP. Nature *365*, 855-859.
1243 Cirelli, C., and Tononi, G. (1998). Changes in anti-phosphoserine and anti-phosphothreonine
1244 antibody binding during the sleep-waking cycle and after lesions of the locus coeruleus. Sleep
1245 Research Online : SRO *1*, 11-18.
1246 Comb, M., Birnberg, N.C., Seasholtz, A., Herbert, E., and Goodman, H.M. (1986). A cyclic AMP-
1247 and phorbol ester-inducible DNA element. Nature *323*, 353-356.
1248 Conkright, M.D., Canettieri, G., Screaton, R., Guzman, E., Miraglia, L., Hogenesch, J.B., and
1249 Montminy, M. (2003). TORCs: transducers of regulated CREB activity. Molecular Cell *12*, 413-
1250 423.
1251 Dash, P.K., Hochner, B., and Kandel, E.R. (1990). Injection of the cAMP-responsive element into
1252 the nucleus of Aplysia sensory neurons blocks long-term facilitation. Nature *345*, 718-721.

1253 de la Cova, C., Abril, M., Bellosta, P., Gallant, P., and Johnston, L.A. (2004). Drosophila myc
1254 regulates organ size by inducing cell competition. Cell *117*, 107-116.
1255 de Vivo, L., Bellesi, M., Marshall, W., Bushong, E.A., Ellisman, M.H., Tononi, G., and Cirelli, C.
1256 (2017). Ultrastructural evidence for synaptic scaling across the wake/sleep cycle. Science *355*, 507-
1257 510.
1258 Deverman, B.E., Pravdo, P.L., Simpson, B.P., Kumar, S.R., Chan, K.Y., Banerjee, A., Wu, W.L.,
1259 Yang, B., Huber, N., Pasca, S.P.*, et al.* (2016). Cre-dependent selection yields AAV variants for
1260 widespread gene transfer to the adult brain. Nature Biotechnology *34*, 204-209.
1261 Dickinson, M.E., Flenniken, A.M., Ji, X., Teboul, L., Wong, M.D., White, J.K., Meehan, T.F.,
1262 Weninger, W.J., Westerberg, H., Adissu, H.*, et al.* (2016). High-throughput discovery of novel
1263 developmental phenotypes. Nature *537*, 508-514.
1264 Diering, G.H., Nirujogi, R.S., Roth, R.H., Worley, P.F., Pandey, A., and Huganir, R.L. (2017).
1265 Homer1a drives homeostatic scaling-down of excitatory synapses during sleep. Science *355*, 511-
1266 515.
1267 Donlea, J.M., Ramanan, N., and Shaw, P.J. (2009). Use-dependent plasticity in clock neurons
1268 regulates sleep need in Drosophila. Science *324*, 105-108.
1269 Elliott, A.S., Huber, J.D., O'Callaghan, J.P., Rosen, C.L., and Miller, D.B. (2014). A review of
1270 sleep deprivation studies evaluating the brain transcriptome. SpringerPlus *3*, 728.
1271 Fisher, S.P., Godinho, S.I., Pothecary, C.A., Hankins, M.W., Foster, R.G., and Peirson, S.N. (2012).
1272 Rapid assessment of sleep-wake behavior in mice. Journal of Biological Rhythms *27*, 48-58.
1273 Flavell, S.W., Cowan, C.W., Kim, T.K., Greer, P.L., Lin, Y., Paradis, S., Griffith, E.C., Hu, L.S.,
1274 Chen, C., and Greenberg, M.E. (2006). Activity-dependent regulation of MEF2 transcription
1275 factors suppresses excitatory synapse number. Science *311*, 1008-1012.

1276 Flores, A.E., Flores, J.E., Deshpande, H., Picazo, J.A., Xie, X.S., Franken, P., Heller, H.C., Grahn,
1277 D.A., and O'Hara, B.F. (2007). Pattern recognition of sleep in rodents using piezoelectric signals
1278 generated by gross body movements. IEEE Transactions on Bio-medical Engineering *54*, 225-233.
1279 Foust, K.D., Nurre, E., Montgomery, C.L., Hernandez, A., Chan, C.M., and Kaspar, B.K. (2009).
1280 Intravascular AAV9 preferentially targets neonatal neurons and adult astrocytes. Nature
1281 Biotechnology *27*, 59-65.
1282 Franken, P., Chollet, D., and Tafti, M. (2001). The homeostatic regulation of sleep need is under
1283 genetic control. Journal of Neuroscience *21*, 2610-2621.
1284 Funato, H., Miyoshi, C., Fujiyama, T., Kanda, T., Sato, M., Wang, Z., Ma, J., Nakane, S., Tomita,
1285 J., Ikkyu, A.*, et al.* (2016). Forward-genetics analysis of sleep in randomly mutagenized mice.
1286 Nature *539*, 378-383.
1287 Ganguly-Fitzgerald, I., Donlea, J., and Shaw, P.J. (2006). Waking experience affects sleep need in
1288 Drosophila. Science *313*, 1775-1781.
1289 Gierut, J.J., Jacks, T.E., and Haigis, K.M. (2014). Strategies to achieve conditional gene mutation
1290 in mice. Cold Spring Harbor Protocols *2014*, 339-349.
1291 Gonzalez, G.A., and Montminy, M.R. (1989). Cyclic AMP stimulates somatostatin gene
1292 transcription by phosphorylation of CREB at serine 133. Cell *59*, 675-680.
1293 Gradinaru, V. (2020). Expanding the brain researcher's toolkit. Science *369*, 637.
1294 Graves, L.A., Hellman, K., Veasey, S., Blendy, J.A., Pack, A.I., and Abel, T. (2003). Genetic
1295 evidence for a role of CREB in sustained cortical arousal. Journal of Neurophysiology *90*, 1152-
1296 1159.
1297 Harvey, K.F., Pfleger, C.M., and Hariharan, I.K. (2003). The Drosophila Mst ortholog, hippo,
1298 restricts growth and cell proliferation and promotes apoptosis. Cell *114*, 457-467.
1299 Hellman, K., Hernandez, P., Park, A., and Abel, T. (2010). Genetic evidence for a role for protein
1300 kinase A in the maintenance of sleep and thalamocortical oscillations. Sleep *33*, 19-28.

1301 Hocquemiller, M., Giersch, L., Audrain, M., Parker, S., and Cartier, N. (2016). Adeno-Associated
1302 Virus-Based Gene Therapy for CNS Diseases. Human Gene Therapy *27*, 478-496.
1303 Honda, T., Fujiyama, T., Miyoshi, C., Ikkyu, A., Hotta-Hirashima, N., Kanno, S., Mizuno, S.,
1304 Sugiyama, F., Takahashi, S., Funato, H.*, et al.* (2018). A single phosphorylation site of SIK3
1305 regulates daily sleep amounts and sleep need in mice. Proceedings of the National Academy of
1306 Sciences of the United States of America *115*, 10458-10463.
1307 Hsu, P.D., Lander, E.S., and Zhang, F. (2014). Development and applications of CRISPR-Cas9 for
1308 genome engineering. Cell *157*, 1262-1278.
1309 Hu, J.H., Park, J.M., Park, S., Xiao, B., Dehoff, M.H., Kim, S., Hayashi, T., Schwarz, M.K.,
1310 Huganir, R.L., Seeburg, P.H.*, et al.* (2010). Homeostatic scaling requires group I mGluR activation
1311 mediated by Homer1a. Neuron *68*, 1128-1142.
1312 Huang, H., Potter, C.J., Tao, W., Li, D.M., Brogiolo, W., Hafen, E., Sun, H., and Xu, T. (1999).
1313 PTEN affects cell size, cell proliferation and apoptosis during Drosophila eye development.
1314 Development *126*, 5365-5372.
1315 Huber, R., Ghilardi, M.F., Massimini, M., Ferrarelli, F., Riedner, B.A., Peterson, M.J., and Tononi,
1316 G. (2006). Arm immobilization causes cortical plastic changes and locally decreases sleep slow
1317 wave activity. Nature Neuroscience *9*, 1169-1176.
1318 Huber, R., Ghilardi, M.F., Massimini, M., and Tononi, G. (2004). Local sleep and learning. Nature
1319 *430*, 78-81.
1320 Ibata, K., Sun, Q., and Turrigiano, G.G. (2008). Rapid synaptic scaling induced by changes in
1321 postsynaptic firing. Neuron *57*, 819-826.
1322 Iourgenko, V., Zhang, W., Mickanin, C., Daly, I., Jiang, C., Hexham, J.M., Orth, A.P., Miraglia, L.,
1323 Meltzer, J., Garza, D.*, et al.* (2003). Identification of a family of cAMP response element-binding
1324 protein coactivators by genome-scale functional analysis in mammalian cells. Proceedings of the
1325 National Academy of Sciences of the United States of America *100*, 12147-12152.

1326 Jinek, M., Chylinski, K., Fonfara, I., Hauer, M., Doudna, J.A., and Charpentier, E. (2012). A
1327 programmable dual-RNA-guided DNA endonuclease in adaptive bacterial immunity. Science *337*,
1328 816-821.
1329 Kalogiannis, M., Grupke, S.L., Potter, P.E., Edwards, J.G., Chemelli, R.M., Kisanuki, Y.Y.,
1330 Yanagisawa, M., and Leonard, C.S. (2010). Narcoleptic orexin receptor knockout mice express
1331 enhanced cholinergic properties in laterodorsal tegmental neurons. The European Journal of
1332 Neuroscience *32*, 130-142.
1333 Kandel, E.R. (2012). The molecular biology of memory: cAMP, PKA, CRE, CREB-1, CREB-2,
1334 and CPEB. Molecular Brain *5*, 14.
1335 Kapfhamer, D., Valladares, O., Sun, Y., Nolan, P.M., Rux, J.J., Arnold, S.E., Veasey, S.C., and
1336 Bucan, M. (2002). Mutations in Rab3a alter circadian period and homeostatic response to sleep loss
1337 in the mouse. Nature Genetics *32*, 290-295.
1338 Kaplitt, M.G., Feigin, A., Tang, C., Fitzsimons, H.L., Mattis, P., Lawlor, P.A., Bland, R.J., Young,
1339 D., Strybing, K., Eidelberg, D.*, et al.* (2007). Safety and tolerability of gene therapy with an adeno-
1340 associated virus (AAV) borne GAD gene for Parkinson's disease: an open label, phase I trial.
1341 Lancet *369*, 2097-2105.
1342 Katoh, Y., Takemori, H., Lin, X.Z., Tamura, M., Muraoka, M., Satoh, T., Tsuchiya, Y., Min, L.,
1343 Doi, J., Miyauchi, A.*, et al.* (2006). Silencing the constitutive active transcription factor CREB by
1344 the LKB1-SIK signaling cascade. The FEBS Journal *273*, 2730-2748.
1345 Kohlmeier, K.A., Tyler, C.J., Kalogiannis, M., Ishibashi, M., Kristensen, M.P., Gumenchuk, I.,
1346 Chemelli, R.M., Kisanuki, Y.Y., Yanagisawa, M., and Leonard, C.S. (2013). Differential actions of
1347 orexin receptors in brainstem cholinergic and monoaminergic neurons revealed by receptor
1348 knockouts: implications for orexinergic signaling in arousal and narcolepsy. Frontiers in
1349 Neuroscience *7*, 246.

1350 Konermann, S., Lotfy, P., Brideau, N.J., Oki, J., Shokhirev, M.N., and Hsu, P.D. (2018).
1351 Transcriptome Engineering with RNA-Targeting Type VI-D CRISPR Effectors. Cell *173*, 665-676
1352 e614.
1353 Lao, Z., Raju, G.P., Bai, C.B., and Joyner, A.L. (2012). MASTR: a technique for mosaic mutant
1354 analysis with spatial and temporal control of recombination using conditional floxed alleles in mice.
1355 Cell Reports *2*, 386-396.
1356 Lee, T., and Luo, L. (1999). Mosaic analysis with a repressible cell marker for studies of gene
1357 function in neuronal morphogenesis. Neuron *22*, 451-461.
1358 Li, W., and Baker, N.E. (2007). Engulfment is required for cell competition. Cell *129*, 1215-1225.
1359 Lisman, J., Yasuda, R., and Raghavachari, S. (2012). Mechanisms of CaMKII action in long-term
1360 potentiation. Nature Reviews Neuroscience *13*, 169-182.
1361 Liu, D., and Dan, Y. (2019). A Motor Theory of Sleep-Wake Control: Arousal-Action Circuit.
1362 Annual Review of Neuroscience *42*, 27-46.
1363 Lo, C.C., Chou, T., Penzel, T., Scammell, T.E., Strecker, R.E., Stanley, H.E., and Ivanov, P. (2004).
1364 Common scale-invariant patterns of sleep-wake transitions across mammalian species. Proceedings
1365 of the National Academy of Sciences of the United States of America *101*, 17545-17548.
1366 Marchio, S., Sidman, R.L., Arap, W., and Pasqualini, R. (2016). Brain endothelial cell-targeted
1367 gene therapy of neurovascular disorders. EMBO Molecular Medicine *8*, 592-594.
1368 Mikhail, C., Vaucher, A., Jimenez, S., and Tafti, M. (2017). ERK signaling pathway regulates sleep
1369 duration through activity-induced gene expression during wakefulness. Science Signaling *10*.
1370 Montminy, M.R., Sevarino, K.A., Wagner, J.A., Mandel, G., and Goodman, R.H. (1986).
1371 Identification of a cyclic-AMP-responsive element within the rat somatostatin gene. Proceedings of
1372 the National Academy of Sciences of the United States of America *83*, 6682-6686.
1373 Moreno, E., and Basler, K. (2004). dMyc transforms cells into super-competitors. Cell *117*, 117-
1374 129.

1375 Moresco, E.M., Li, X., and Beutler, B. (2013). Going forward with genetics: recent technological
1376 advances and forward genetics in mice. The American Journal of Pathology *182*, 1462-1473.
1377 Muzumdar, M.D., Luo, L., and Zong, H. (2007). Modeling sporadic loss of heterozygosity in mice
1378 by using mosaic analysis with double markers (MADM). Proceedings of the National Academy of
1379 Sciences of the United States of America *104*, 4495-4500.
1380 Nonaka, M., Kim, R., Fukushima, H., Sasaki, K., Suzuki, K., Okamura, M., Ishii, Y., Kawashima,
1381 T., Kamijo, S., Takemoto-Kimura, S.*, et al.* (2014). Region-specific activation of CRTC1-CREB
1382 signaling mediates long-term fear memory. Neuron *84*, 92-106.
1383 Oishi, Y., Williams, R.H., Agostinelli, L., Arrigoni, E., Fuller, P.M., Mochizuki, T., Saper, C.B.,
1384 and Scammell, T.E. (2013). Role of the medial prefrontal cortex in cataplexy. Journal of
1385 Neuroscience *33*, 9743-9751.
1386 Ojala, D.S., Amara, D.P., and Schaffer, D.V. (2015). Adeno-associated virus vectors and
1387 neurological gene therapy. The Neuroscientist *21*, 84-98.
1388 Pack, A.I., Galante, R.J., Maislin, G., Cater, J., Metaxas, D., Lu, S., Zhang, L., Von Smith, R., Kay,
1389 T., Lian, J.*, et al.* (2007). Novel method for high-throughput phenotyping of sleep in mice.
1390 Physiological Genomics *28*, 232-238.
1391 Pagliarini, R.A., and Xu, T. (2003). A genetic screen in Drosophila for metastatic behavior. Science
1392 *302*, 1227-1231.
1393 Pardo, L., Valor, L.M., Eraso-Pichot, A., Barco, A., Golbano, A., Hardingham, G.E., Masgrau, R.,
1394 and Galea, E. (2017). CREB Regulates Distinct Adaptive Transcriptional Programs in Astrocytes
1395 and Neurons. Scientific Reports *7*, 6390.
1396 Plath, N., Ohana, O., Dammermann, B., Errington, M.L., Schmitz, D., Gross, C., Mao, X.,
1397 Engelsberg, A., Mahlke, C., Welzl, H.*, et al.* (2006). Arc/Arg3.1 is essential for the consolidation
1398 of synaptic plasticity and memories. Neuron *52*, 437-444.

1399 Port, F., Strein, C., Stricker, M., Rauscher, B., Heigwer, F., Zhou, J., Beyersdorffer, C., Frei, J.,
1400 Hess, A., Kern, K., *et al.* (2020). A large-scale resource for tissue-specific CRISPR mutagenesis in
1401 Drosophila. eLife *9*.
1402 Potter, C.J., Huang, H., and Xu, T. (2001). Drosophila Tsc1 functions with Tsc2 to antagonize
1403 insulin signaling in regulating cell growth, cell proliferation, and organ size. Cell *105*, 357-368.
1404 Pulicherla, N., Shen, S., Yadav, S., Debbink, K., Govindasamy, L., Agbandje-McKenna, M., and
1405 Asokan, A. (2011). Engineering liver-detargeted AAV9 vectors for cardiac and musculoskeletal
1406 gene transfer. Molecular Therapy *19*, 1070-1078.
1407 Rechtschaffen, A., Bergmann, B.M., Everson, C.A., Kushida, C.A., and Gilliland, M.A. (1989).
1408 Sleep deprivation in the rat: X. Integration and discussion of the findings. Sleep *12*, 68-87.
1409 Ruppert, S., Cole, T.J., Boshart, M., Schmid, E., and Schutz, G. (1992). Multiple mRNA isoforms
1410 of the transcription activator protein CREB: generation by alternative splicing and specific
1411 expression in primary spermatocytes. The EMBO Journal *11*, 1503-1512.
1412 Sanjana, N.E., Shalem, O., and Zhang, F. (2014). Improved vectors and genome-wide libraries for
1413 CRISPR screening. Nature Methods *11*, 783-784.
1414 Saper, C.B., Fuller, P.M., Pedersen, N.P., Lu, J., and Scammell, T.E. (2010). Sleep state switching.
1415 Neuron *68*, 1023-1042.
1416 Saper, C.B., Scammell, T.E., and Lu, J. (2005). Hypothalamic regulation of sleep and circadian
1417 rhythms. Nature *437*, 1257-1263.
1418 Seeburg, D.P., Feliu-Mojer, M., Gaiottino, J., Pak, D.T., and Sheng, M. (2008). Critical role of
1419 CDK5 and Polo-like kinase 2 in homeostatic synaptic plasticity during elevated activity. Neuron *58*,
1420 571-583.
1421 Shaw, P.J., Tononi, G., Greenspan, R.J., and Robinson, D.F. (2002). Stress response genes protect
1422 against lethal effects of sleep deprivation in Drosophila. Nature *417*, 287-291.

1423 Shaywitz, A.J., and Greenberg, M.E. (1999). CREB: a stimulus-induced transcription factor
1424 activated by a diverse array of extracellular signals. Annual Review of Biochemistry *68*, 821-861.
1425 Shepherd, J.D., Rumbaugh, G., Wu, J., Chowdhury, S., Plath, N., Kuhl, D., Huganir, R.L., and
1426 Worley, P.F. (2006). Arc/Arg3.1 mediates homeostatic synaptic scaling of AMPA receptors.
1427 Neuron *52*, 475-484.
1428 Short, J.M., Wynshaw-Boris, A., Short, H.P., and Hanson, R.W. (1986). Characterization of the
1429 phosphoenolpyruvate carboxykinase (GTP) promoter-regulatory region. II. Identification of cAMP
1430 and glucocorticoid regulatory domains. The Journal of Biological Chemistry *261*, 9721-9726.
1431 Sunagawa, G.A., Sumiyama, K., Ukai-Tadenuma, M., Perrin, D., Fujishima, H., Ukai, H.,
1432 Nishimura, O., Shi, S., Ohno, R.I., Narumi, R.*, et al.* (2016). Mammalian Reverse Genetics without
1433 Crossing Reveals Nr3a as a Short-Sleeper Gene. Cell Reports *14*, 662-677.
1434 Suzuki, K., Tsunekawa, Y., Hernandez-Benitez, R., Wu, J., Zhu, J., Kim, E.J., Hatanaka, F.,
1435 Yamamoto, M., Araoka, T., Li, Z.*, et al.* (2016). In vivo genome editing via CRISPR/Cas9
1436 mediated homology-independent targeted integration. Nature *540*, 144-149.
1437 Takahashi, J.S., Pinto, L.H., and Vitaterna, M.H. (1994). Forward and reverse genetic approaches
1438 to behavior in the mouse. Science *264*, 1724-1733.
1439 Tatsuki, F., Sunagawa, G.A., Shi, S., Susaki, E.A., Yukinaga, H., Perrin, D., Sumiyama, K., Ukai-
1440 Tadenuma, M., Fujishima, H., Ohno, R.*, et al.* (2016). Involvement of Ca(2+)-Dependent
1441 Hyperpolarization in Sleep Duration in Mammals. Neuron *90*, 70-85.
1442 Tian, D., Wenlock, S., Kabir, M., Tzotzos, G., Doig, A.J., and Hentges, K.E. (2018). Identifying
1443 mouse developmental essential genes using machine learning. Disease Models & Mechanisms *11*.
1444 Tononi, G., and Cirelli, C. (2014). Sleep and the price of plasticity: from synaptic and cellular
1445 homeostasis to memory consolidation and integration. Neuron *81*, 12-34.

1446 Vaccaro, A., Kaplan Dor, Y., Nambara, K., Pollina, E.A., Lin, C., Greenberg, M.E., and Rogulja, D.
1447 (2020). Sleep Loss Can Cause Death through Accumulation of Reactive Oxygen Species in the Gut.
1448 Cell *181*, 1307-1328 e1315.
1449 Wang, H., Yang, H., Shivalila, C.S., Dawlaty, M.M., Cheng, A.W., Zhang, F., and Jaenisch, R.
1450 (2013). One-step generation of mice carrying mutations in multiple genes by CRISPR/Cas-
1451 mediated genome engineering. Cell *153*, 910-918.
1452 Wang, W., Warren, M., and Bradley, A. (2007). Induced mitotic recombination of p53 in vivo.
1453 Proceedings of the National Academy of Sciences of the United States of America *104*, 4501-4505.
1454 Wang, Z., Ma, J., Miyoshi, C., Li, Y., Sato, M., Ogawa, Y., Lou, T., Ma, C., Gao, X., Lee, C.*, et al.*
1455 (2018). Quantitative phosphoproteomic analysis of the molecular substrates of sleep need. Nature
1456 *558*, 435-439.
1457 Weber, F., and Dan, Y. (2016). Circuit-based interrogation of sleep control. Nature *538*, 51-59.
1458 Weiergraber, M., Henry, M., Hescheler, J., Smyth, N., and Schneider, T. (2005).
1459 Electrocorticographic and deep intracerebral EEG recording in mice using a telemetry system.
1460 Brain Research Brain Research Protocols *14*, 154-164.
1461 Wimmer, M., Cui, R., Blackwell, J., and Abel, T. (2020). CREB is Required in Excitatory Neurons
1462 in the Forebrain to Sustain Wakefulness. Sleep, zsaa267.
1463 Wu, Z., Asokan, A., and Samulski, R.J. (2006). Adeno-associated virus serotypes: vector toolkit for
1464 human gene therapy. Molecular Therapy *14*, 316-327.
1465 Xie, K., Minkenberg, B., and Yang, Y. (2015). Boosting CRISPR/Cas9 multiplex editing capability
1466 with the endogenous tRNA-processing system. Proceedings of the National Academy of Sciences
1467 of the United States of America *112*, 3570-3575.
1468 Xie, T., and Spradling, A.C. (1998). decapentaplegic is essential for the maintenance and division
1469 of germline stem cells in the Drosophila ovary. Cell *94*, 251-260.

1470 Xu, T., and Rubin, G.M. (1993). Analysis of genetic mosaics in developing and adult Drosophila
1471 tissues. Development *117*, 1223-1237.
1472 Xu, T., Wang, W., Zhang, S., Stewart, R.A., and Yu, W. (1995). Identifying tumor suppressors in
1473 genetic mosaics: the Drosophila lats gene encodes a putative protein kinase. Development *121*,
1474 1053-1063.
1475 Yaghouby, F., Donohue, K.D., O'Hara, B.F., and Sunderam, S. (2016). Noninvasive dissection of
1476 mouse sleep using a piezoelectric motion sensor. Journal of Neuroscience Methods *259*, 90-100.
1477 Yang, Y., Wang, L., Bell, P., McMenamin, D., He, Z., White, J., Yu, H., Xu, C., Morizono, H.,
1478 Musunuru, K.*, et al.* (2016). A dual AAV system enables the Cas9-mediated correction of a
1479 metabolic liver disease in newborn mice. Nature Biotechnology *34*, 334-338.
1480 Yin, L., Maddison, L.A., Li, M., Kara, N., LaFave, M.C., Varshney, G.K., Burgess, S.M., Patton,
1481 J.G., and Chen, W. (2015). Multiplex Conditional Mutagenesis Using Transgenic Expression of
1482 Cas9 and sgRNAs. Genetics *200*, 431-441.
1483 Yochem, J., and Herman, R.K. (2003). Investigating C. elegans development through mosaic
1484 analysis. Development *130*, 4761-4768.
1485 Zetsche, B., Heidenreich, M., Mohanraju, P., Fedorova, I., Kneppers, J., DeGennaro, E.M.,
1486 Winblad, N., Choudhury, S.R., Abudayyeh, O.O., Gootenberg, J.S.*, et al.* (2017). Multiplex gene
1487 editing by CRISPR-Cpf1 using a single crRNA array. Nature Biotechnology *35*, 31-34.
1488 Zhong, G., Wang, H., Li, Y., Tran, M.H., and Farzan, M. (2017). Cpf1 proteins excise CRISPR
1489 RNAs from mRNA transcripts in mammalian cells. Nature Chemical Biology *13*, 839-841.
1490 Zong, H., Espinosa, J.S., Su, H.H., Muzumdar, M.D., and Luo, L. (2005). Mosaic analysis with
1491 double markers in mice. Cell *121*, 479-492.
1492
1493